uOttawa

L'Université canadienne
Canada's university

FACULTÉ DES ÉTUDES SUPÉRIEURES ET POSTOCTORALES

uOttawa

L'Université canadienne
Canada's university

FACULTY OF GRADUATE AND POSDOCTORAL STUDIES

Jaime Corinaldi
AUTEUR DE LA THÈSE / AUTHOR OF THESIS

M.Sc. (Cellular and Molecular Medicine)
GRADE / DEGREE

Department of Cellular and Molecular Medicine
FACULTÉ, ÉCOLE, DÉPARTEMENT / FACULTY, SCHOOL, DEPARTMENT

Troglitazone Induces Extracellular Matrix & Cytoskeleton Remodeling in the IMCD-K2 & M1 Renal Collecting Duct Cell Lines

TITRE DE LA THÈSE / TITLE OF THESIS

R. Hebert
DIRECTEUR (DIRECTRICE) DE LA THÈSE / THESIS SUPERVISOR

CO-DIRECTEUR (CO-DIRECTRICE) DE LA THÈSE / THESIS CO-SUPERVISOR

EXAMINATEURS (EXAMINATRICES) DE LA THÈSE / THESIS EXAMINERS

C. Kennedy

D. Lohnes

Gary W. Slater
Le Doyen de la Faculté des études supérieures et postdoctorales / Dean of the Faculty of Graduate and Postdoctoral Studies

TROGLITAZONE INDUCES EXTRACELLULAR MATRIX & CYTOSKELETON REMODELING IN THE IMCD-K2 & M1 RENAL COLLECTING DUCT CELL LINES

Jaime Corinaldi

This thesis is submitted as a partial fulfillment of the M.Sc. program in Cellular Molecular Medicine

September 19th, 2008

University of Ottawa / Kidney Research Center

Ottawa, Ontario

Your file Votre référence
ISBN: 978-0-494-52345-2
Our file Notre référence
ISBN: 978-0-494-52345-2

Abstract

TGF-β activation has been inhibited with Troglitazone, a synthetic PPARγ ligand (Peng, Liu et al. 2006). The fibrotic response in the collecting ducts of the nephron, particularly in terms of EMT, has only recently been established (Ivanova, Butt et al. 2008). The purpose of this study was to characterize a fibrotic response in the collecting duct with TGF-β and to assess PPARγ's role in the phenomenon. We hypothesized PPARγ activation will have a protective effect in the collecting duct, preventing TGF-β mediated EMT. TGF-β was unable to initiate a fibrotic response in the IMCD-K2 & M1 collecting duct cell lines. In contrast, Troglitazone caused morphological changes and decreases in E-cadherin, α-catenin & β-catenin, as well as an increase in fibronectin. These effects were not reversed with PPARγ antagonists or a GSK-3β blocker. Troglitazone induced a transformation in M1 & IMCD-K2 cells independently of PPARγ.

Table of Contents

List of Tables

List of Figures

List of Abbreviations

α-SMA	α Smooth Muscle Actin
ADH	Antidiuretic hormone
AF-1	Activating Factor 1
AF-2	Activating Factor 2
AQP	Aquaporins
BMP	Bone morphogenic protein
BSA	Bovine serum albumin
CBD	Catenin Binding Domain
CCD	Cortical Collecting Duct
CD	Collecting Duct
CTGF	Connective Tissue Growth Factor
DAPI	4',6-diamidino-2-phenylindole
DBD	DNA Binding Domain
DCFDA	2´-7´-dichlorofluorescin diacetate
DMEM	Dulbecco's modified Eagle's medium
DMSO	Dimethyl sulfoxide
ECM	Extracellular matrix
EMT	Epithelial to Mesenchymal Transformation
ERK	Extracellular signal-regulated kinase
FBS	Fetal bovine serum
FN	Fibronectin
GSK-3	Glycogen synthase kinase 3
HAT	Histone acetyl transferase
HDAC	Histone deacetylase
HDL	High density lipoprotein
HGF	Hepatocyte growth factor
IC50	50% inhibitory concentration
IF	Interstitial Fibrosis
IGF	Insulin-like Growth Factor
IMCD	Inner Medullar Collecting Duct
LBD	Ligand Binding Domain
LDL	Low density lipid
LEF	Lymphocyte enhancer factor
LiCl	Lithium Chloride
MAPK	Mitogen-activated protein kinase
MMP	Matrix Metalloprotein
NSAID	Non steroidal anti-inflammatory drug
O/N	Overnight
PBS	Phosphate buffered saline
PCR	Polymerase chain reaction

PGD_2	Prostaglandin E2
PGJ_2	15-deoxy-Δ12,14-prostaglandin J2
PPAR	Peroxisome proliferator-activated receptor
PPRE	Peroxisome Proliferator Response Element
PT	Proximal Tubule
PUFA	Polyunsaturated fatty acid
ROS	Reactive Oxygen Species
RT	Reverse transcriptase
RXR	Retinoid X Receptor
SDS-PAGE	Sodium dodecyl sulphate-polyacrylamide gel electrophoresis
SEM	Standard error of the mean
TBS-T	Tris buffered saline-Tween 20
TBM	Tubular basement membrane
TCF	T-cell factor
TGF-β	Transforming Growth Factor β
TRO	Troglitazone
TZD	Thiazolidinediones
UUO	Unilateral Uereteral Obstruction

Acknowledgements

I would like to thank my family and friends for their continued support, especially my mother Beverley Corinaldi. I would like to thank Dr. John Bell for introducing me to the world of research and Drs. Barbara Vanderhyden and Ken Garson for continuing my passion for research. I would like to thank Dr. Richard Hébert for giving me the opportunity to complete my Master's. I would like to thank my lab members Geneviève Paris, Dr. Rania Nasrallah, Jordan Clark, and Dr. Mona Sadeek for their support and extreme patience during our weekly lab meetings. I would also like to give thanks to the entire kidney research center for creating a pleasant work environment and sharing their knowledge over the last two years. I would also like to give thanks to my committee members, Drs. Kennedy & Scott, for their informative commentary and also to my examination committee, Drs. Kennedy & Lohnes for their patience in reading my thesis.

1.0 Introduction

1.1 Peroxisome proliferator-activated receptors (PPARs)

1.1.1 Molecular Biology

PPARs are ligand-activated transcription factors that heterodimerize with a retinoid X receptor (RXR) (which bind 9-cis retinoic acid) and translocate to the nucleus upon binding of a ligand (Guan, Zhang et al. 1997). The PPAR-RXR duplex recruits multiple coactivating or corepressing cofactors, forming a transcription complex. This complex specifically targets the peroxisome proliferator response element (PPRE) [AGGTCA-AGGTCA] present throughout the genome, particularly in many metabolically relevant genes (Ide, Egan et al. 2003). The expression of these genes can be either induced or repressed depending on the subunits of the PPAR transcription complex and the gene being targeted. All three PPAR genes contain a DNA binding domain (DBD) and a ligand binding domain (LBD), as illustrated in Fig. 1, and each is responsive to a particular group of compounds (Ahmed, Ziouzenkova et al. 2007), (Brown and Plutzky 2007), (Kota, Huang et al. 2005), (Michalik, Auwerx et al. 2006).

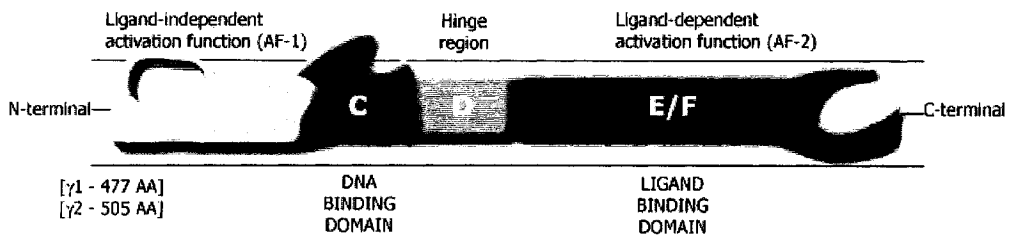

Fig. 1 - *PPAR conserved molecular structure*

The structure of PPARs consists of four functional domains like most nuclear hormone receptors, with a poorly conserved N-terminal A/B region containing the Activating Factor 1 (AF1) ligand-independent transactivation domain. The C region with a twin zinc finger DNA binding domain (DBD), the D domain and its DBD carboxy-terminal extension, E and F regions with a large and flexible ligand binding site, and Activating Factor 2 (AF2) ligand-dependent transactivation domain at the extreme C terminus which also provides the dimerization site (Berger and Wagner 2002).

1.1.2 PPAR Overview

There are currently three cloned PPARs (α, γ, β/δ), all of which are expressed in different tissues at various levels and are involved in numerous cellular events including metabolism, differentiation, growth, apoptosis, and tumorigenesis (Chou, Wang et al. 2007), (Han, Kim et al. 2007), (Panchapakesan, Sumual et al. 2005). The fibrate receptor PPARα is highly expressed in metabolically active tissues: skeletal muscle, liver, heart, kidney, and brown adipose tissue. The PPAR alpha agonist fenofibrate has been shown to attenuate low density lipid (LDL) and triglyceride levels in hypertension as its activation increases high density lipoprotein (HDL) cholesterol synthesis (Hansen 1999). PPAR alpha's protective role in cardiovascular complications may be due to the fact it is a key regulator of fatty acid oxidation genes with protein levels of essential enzymes in the β-oxidation pathway increasing as a result of PPARα activation (Djouadi and Bastin 2001).

Deleted: (Chou, Wang et al. 2007)

Obesity has been treated with the PPAR delta agonist GW501516 as it is known to induce β-oxidation in adipose tissue reducing the overall level of fatty cells and normalizing many metabolic parameters.

This increased fatty acid catabolism & energy uncoupling was also observed in muscle tissue (Barish, Narkar et al. 2006). This increase in metabolic activity has been shown to reduce and possibly reverse some symptoms of diabetes and diabetic nephropathy (Berger and Wagner 2002). PPARβ/δ is the most ubiquitously expressed isoform, and is the intracrine target for PGI_2 and PGE_2. PPARδ has been shown to improve hypertriglyceridemia and insulin resistance, as well as the suppression of macrophage-related inflammation, emphasizing its potential as a therapeutic target in combating metabolic disease.

The glitazone receptor PPARγ is abundant in the brown adipose tissue, intestine, spleen, and is found in the kidney where its expression levels, as well as those of its endogenous ligand 15d-prostaglandin J_2 (PGJ_2), an active metabolite of prostaglandin D_2 (PGD_2), are high. Two isoforms of PPARγ, $PPAR\gamma_1$ and $PPAR\gamma_2$, are generated by alternative splicing with $PPAR\gamma_2$ having an additional 30 amino acids at the amino terminus. $PPAR\gamma_2$ is predominantly expressed in adipose tissue and has been identified as the first adipocyte-specific transcription factor (Tontonoz, Hu et al. 1994). A third form, $PPAR\gamma_3$, has been detected in humans and is transcribed from alternative promoter usage. PPARγ3 mRNA expression was restricted to adipose tissue and large intestine and has been shown to have a role in regulating the control of height and lipid homeostasis (Fajas, Fruchart et al. 1998).

1.1.3 Mechanism

The overall PPAR-mediated effect on target genes is dependent upon several regulatory elements including the nature of the ligand, phosphorylation of the receptor, and the recruitment of co-repressors or co-activators (i.e. cAMP, CREB). Fig. 2 illustrates the mechanism of

action for PPARγ. Interestingly, similar to PPARs, their heterodimerization partner RXR exists as three distinct isoforms: RXRα, β, and γ, all of which are activated by the agonist 9-*cis* retinoic acid. No specific roles have yet been elaborated for these different isoforms within the PPAR:RXR complex however, synthetic RXR agonists (rexinoids) can activate the complex and thereby obtain antidiabetic outcomes similar to those seen with PPAR agonists in mouse models of type 2 diabetes (Berger and Wagner 2002). This may prove to be an interesting field of research to further our understanding of PPAR function and action.

Fig. 2 - *PPAR Ligand Binding & Transcription Complex Formation.*

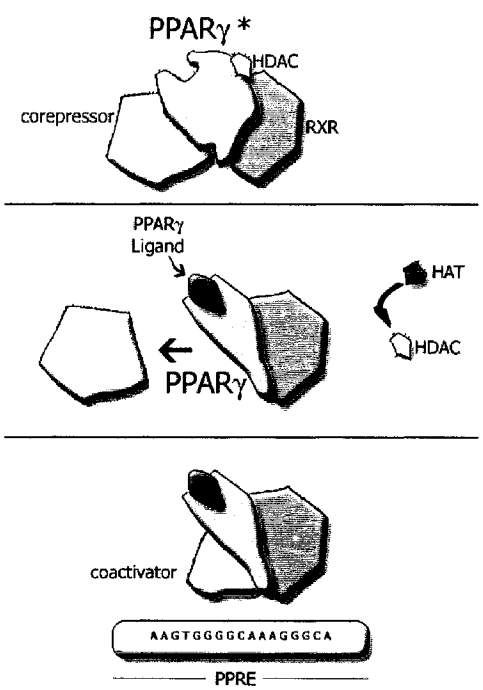

In terms of PPARγ specifically, ligand binding induces a conformational change in a conserved AF2 helix in the carboxyl terminus of the ligand binding domain. This helix is the site of interaction for several coactivators that stimulate transcription *via* acetylation of core histones or interaction with the basal transcription machinery. PPARγ phosphorylation results in a reduction in receptor activity partially through the resulting hindrance of ligand binding (Kumar and Thompson 1999).

Certain nuclear receptors have been shown to integrate their ligand signals into the histone code through histone acetylation or deacetylation (Takada, Mihara et al. 2007). In a non-ligand bound state, nuclear receptors are transcriptionally inactive as they are associated with co-repressor complexes. PPAR co-repressor complexes often contain histone deacetylases (HDAC), resulting in hypoacetylated histone molecules preventing the recruitment of co-activator complex formation. Ligand binding to nuclear receptors can be associated with histone acetyltransferase (HAT) activity as the HDAC co-repressor complexes detach from the PPAR nuclear receptor and allow for transcriptional activity. Ligand independent repression may also play a factor in the regulation of PPAR dependent pathways through complex interactions with multiple transcriptional regulators.

Several PPARγ ligands also stimulate the degradation of PPARγ protein. It has been shown that this degradation is dependent upon the ligand-gated activation function 2 (AF2) domain. Ligand binding and activation of the AF2 domain increase the transcriptional function of PPARγ; this activation however also induces ubiquitination and subsequent degradation of this receptor by the proteasome (Hauser, Adelmant et al. 2000). The result is a feedback system for balancing the transcriptional activity of PPARγ.

1.1.4 Ligands / Antagonists

Synthetic ligands for PPARγ are the aforementioned thiazoliidinediones (troglitazone, pioglitazone, rosiglitazone, ciglitazone) and certain nonsteroidal anti-inflammatory drugs (NSAIDs) (Bishop-Bailey and Warner 2003). Natural ligands include 15-deoxy-prostaglandin J_2 (15-dPGJ_2 or PGJ_2), certain polyunsaturated fatty acids

(PUFAs) such as linoleic acid, and endogenous low density lipoprotein (LDL) particles. Troglitazone is a well studied synthetic PPARγ agonist. It has high specificity for PPARγ as it does not activate the PPARδ or PPARα isoforms at a concentration of 25mM and higher. Troglitazone is a member of a new class of antidiabetic drugs that are currently used to improve insulin sensitivity in type 2 diabetics by enhancing pancreatic islet beta-cell function through increased absorption of fat cells, stimulating the metabolism of glucose thereby reducing the liver's production of new glucose.

Troglitazone is currently under heavy investigation in cancer research where its ability to affect the E-cadherin/β-catenin and Wnt signalling pathway have been characterized (Annicotte, Iankova et al. 2006). It should be noted however that three distinct pathways through which glitazones may act have been identified; one through PPAR dependent pathways, the second through ERK activation, and the third through mitochondrial AMPK activation (Turturro, Oliver et al. 2007). The PPARγ antagonist GW9662 (Cayman Chemicals) binds PPARγ with an IC50 in the nanomolar range, and is 10- and 600-fold less potent in binding PPARα and PPARδ, respectively (Lehmann, Moore et al. 1995). Its antagonistic effects stem from its ability to covalently bind to a cysteine residue (Cys_{285}) in the ligand activation domain, preventing any further binding of ligand thus inhibiting activation (Leesnitzer, Parks et al. 2002). T0070907 was identified as a potent and selective PPARγ antagonist with an apparent binding affinity of 1 nM. T0070907 covalently modifies Cys_{313} of PPARγ, inducing conformational changes that block the recruitment of transcriptional cofactors to the PPARγ/RXR heterodimer (Lee, Elwood et al. 2002).

1.2 Renal Physiology

1.2.1 Overview

Filtration, reabsorption, and secretion are the primary processes involved in kidney function. The functional unit of the kidney, the nephron, filters blood plasma. This process begins in the renal corpuscle, composed of a glomerulus enclosed in a Bowman's capsule. Starling forces drive the ultrafiltration of the blood, removing cells, proteins, and other large molecules. The ultrafiltrate enters Bowman's space and passes through the proximal tubule, the loop of Henle, the distal convoluted tubule, and finally the collecting tubules to form urine (Borke, Costoff et al. 1999).

Hormone secretion is also a vital role of the kidney. The major hormone regulators secreted by the kidneys are erythropoietin, which stimulates bone marrow production of red blood cells; renin which regulates blood pressure; and calcitriol, the active form of vitamin D, which helps maintain calcium for bones and for normal chemical balance in the body; as well as prostaglandins, which play a role in various biological pathways.

1.2.2 Collecting Duct

In the collecting duct specifically aldosterone which stimulates active sodium reabsorption and antidiuretic hormone (ADH) which stimulates passive water reabsorption, play major roles in electrolyte balance and renal dynamics. The collecting duct connects to the ureter and is the final segment of the nephron, accounting for 5% of sodium and water reabsorption (Hoorn, Pisitkun et al. 2008). The collecting ducts, particularly the outer medullary and cortical collecting ducts,

are largely impermeable to water without the presence of ADH. When ADH is present, aquaporins (AQP) allow for the reabsorption of this water, thereby inhibiting diuresis (Hoorn, Pisitkun et al. 2008).

There are two distinct cell types in the collecting duct system, namely, the intercalated cells and the principal cells. The principal cell is responsible for the reabsorption of Na^+, secretion of K^+ and reabsorption of water. Luminal entry of Na^+ is passive and Na^+ and K^+ movements are linked by the basolateral Na^+, K^+- ATPase primary active transport pump. These cells are under the physiological control of aldosterone which acts to increase Na^+ reabsorption and K^+ secretion. It acts to increase the number of Na^+ channels in the luminal membrane and the number of Na^+, K^+-ATPase pumps in the basolateral membrane. Water reabsorption is sensitive to ADH which acts to increase water permeability of the cell by increasing the number of water channels in the luminal membrane (Hoorn, Pisitkun et al. 2008).

Intercalated cells regulate acid-base homeostasis and have two phenotypes. Type α intercalated cells secrete H^+ by a primary active H^+ transporter and a luminal H^+, K^+ antiporter. H^+ secretion plays a major role in reabsorption of HCO_3^- by reacting with filtered HCO_3^-. The secreted H^+ also plays a major role in regeneration of HCO_3^- ion by reacting with various non-bicarbonate urinary buffers. These cells also function in K^+ reabsorption. Type-β intercalated cells function in Cl^- reabsorption and HCO_3^- secretion by a secondary active HCO_3^-, Cl^- antiporter. The activity of this system is sensitive to extracellular fluid pH and Cl^- levels (Borke, Costoff et al. 1999).

1.2.3 PPARγ and the Collecting Duct

Thiazolidinediones are widely used to treat type 2 diabetes mellitus; however, their use is complicated by systemic fluid

retention. Along the nephron, the pharmacological target of TZDs, PPAR γ, is abundant in the collecting duct. Treatment with TZDs, in some cases, resulted in early weight gain from increased total body water. This weight gain was blocked by amiloride, a collecting duct specific diuretic that directly blocks the epithelial sodium channel. Deletion of PPARγ from the collecting duct, using PPARγ $^{flox/flox}$ transgenic mice, prevented the aforementioned edema phenomenon. The pathway underlying the fluid retention associated with TZDs involves a PPAR-dependent increase in the epithelial Na^+ channel (ENaC) expression. Amiloride has been suggested as a potential fluid counterbalance to TZD treatment (Guan, Hao et al. 2005). Table 1 lists several functions of PPARγ indentified in the kidney.

TABLE 1: Renal functions of PPARγ.

Renal Localization	Function
Collecting Duct	Sodium balance and blood pressure (Yang, Michele et al. 1999) (Ito, Nakamura et al. 2006)
Distal Tubule	Regulates fluid retention (Yang, Michele et al. 1999)
Inner medulla	(Yang, Michele et al. 1999)
Kidney fibroblasts	Inhibits ECM production (Panchapakesan, Pollock et al. 2004) Inhibits cell growth and reduces matrix production in human kidney fibroblasts (Zafiriou, Stanners et al. 2005)
Glomeruli	Reduces ECM proteins (Fibronectin, type IV collagen) and TGF-B1, reduces proteinuria Reduces ECM proteins (Fibronectin, type IV collagen) and TGF-B1, reduces proteinuria (Panchapakesan, Pollock et al. 2004)
Proximal Tubule	Anti-proliferative and anti-inflammatory effects to high glucose (Panchapakesan, Sumual et al. 2005) PGJ_2 was shown to promote apoptotic cell death in opossum kidney proximal tubule cells via reactive oxygen species production and inhibition of nuclear factor-κB (Kang, Kwon et al. 2006)

Thick Ascending Limb	(Ito, Nakamura et al. 2006)
Mesangial cells	Antihypertensive and anti-inflammatory properties (Efrati, Berman et al. 2007)
Podocyte	Podocyte injuries and sclerotic conditions. Protective effect against apoptosis and necrosis. Effects mediated by p27 and TGF-βeta expression (Kanjanabuch, Ma et al. 2007)

1.3 Renal Fibrosis

1.3.1 Overview

Fibrosis is the end result of chronic inflammation resulting from tissue injury, infection, and other adverse stimuli. The inflammatory response is targeted in the treatment of fibrotic diseases however there is evidence that the mechanisms responsible for the fibrotic response are distinct from those regulating inflammation. The key cellular mediator of fibrosis is the myofibroblast, which when activated serves as the primary collagen-producing cell. Myofibroblasts are generated from local mesenchymal cells, epithelial and endothelial cells which have transformed into a mesenchymal phenotype (*refer to section 1.3.2*), as well as from circulating fibrocytes that are derived from bone-marrow stem cells (Wynn 2008). Renal fibrosis is defined by the abnormal accumulation of extracellular matrix that replaces normal kidney structures. Renal fibrosis has become recognized as a crucial factor in the prognosis of kidney disease as it occurs regardless of the underlying disease (hypertension, diabetes, infection, inflammation of renal blood vessels and glomeruli, kidney stones, and cysts) and originating segment (renal vessels, glomeruli, tubules) (Yang, Pan et

al. 2006). It has been suggested that a common fibrotic pathway is reached regardless of the initial fibrotic responses.

TGF-β is the primary fibrotic agent promoting extracellular matrix synthesis, apoptosis, and growth arrest. Potential therapeutic strategies are based on attenuating or interrupting the profibrotic response, namely through targeting the TGF-β signalling pathway (Yang, Pan et al. 2006), (Sam, Wanna et al. 2006).

1.3.2 Epithelial to Mesenchymal Transition

EMT can be described as the process in which epithelial cells that function as ion and fluid transporters lose their epithelial polarity, cellular adhesion molecules reorganize their actin cytoskeleton from a cortical bundle formation that supported adhesion molecules into stress fibres containing de novo expressed α-smooth muscle actin (α-SMA) that support migration. EMT is also defined by a disruption in the tubular basement membrane (TBM) and migration into the interstitium where newly formed myofibroblasts synthesize increasing amounts of extracellular matrix (ECM) (Wu, Yang et al. 2007). Epithelial cells form organized cell-cell junctions and adhesions preventing movement of individual cells resulting in a tight epithelial surface. Mesenchymal cells however tend to be highly motile as they lack this level of organization. The transformation of epithelial and mesenchymal cells is an integral component of embryogenesis and normal organ development however the irregular activation of this transition is associated with several diseased states, namely cancer and fibrosis (Javle, Gibbs et al. 2007). Numerous *in vitro* studies have shown that EMT is regulated by growth factors, cytokines, and metalloproteinases (MMPs) that can disrupt the TBM

integrity and TBM composition. Transforming growth factor (TGF) is the main growth factor reported to mediate the initiation and maintenance of the EMT process. EMT requires either transcriptional repression of genes that maintain the epithelial phenotype (e.g. E-cadherin, claudins, occludins, desmoplakin, desmoglein, integrins) and/or transcriptional activation of genes needed for functional myofibroblasts, e.g. Fibronectin, collagen, vimentin, α-SMA (Takeji, Moriyama et al. 2006). An understanding of EMT and its potential reversibility offers new opportunities for arresting or even reversing the progression of chronic renal disease.

EMT or transformation to the mesenchymal phenotype plays an important role in tumor invasion and metastasis. ERK plays a key role in cellular proliferation, differentiation and survival and its inappropriate activation is a common occurrence in human cancers. ERK inhibition has been shown to reduce TGF-β induced EMT *in vitro* (Xie, Law et al. 2004). Phospohorylated ERK has been revealed as an important adverse prognostic marker in resectable pancreatic cancer and a possible target for therapy. *In vitro* data suggest that mesenchymal transformation may correlate with the activation of PI3 kinase and Ras/ERK pathways. An association of p-ERK in resected pancreatic cancer has been established with EMT markers (low E-cadherin, high Fibronectin, and vimentin) (Javle, Gibbs et al. 2007). Phosphorylated Src has also been shown to have an inverse relation to E-cadherin in primary tumor tissues. Elevated levels of p-Src were accompanied by down-regulation of E-cadherin and increased expression of vimentin in epithelial tumor cells. *In vitro* inhibition of Src led to E-cadherin re-expression and increased cell contact in squamous carcinoma cell lines (Mandal, Myers et al. 2008).

1.3.3 Mesenchymal and ECM Markers

Fibronectin is a multifunctional, ECM glycoprotein composed of two nearly identical disulfide-bound polypeptides with a molecular weight of 220 kDa. Numerous studies have shown that Fibronectin may enhance cell adhesion and cell migration both *in vivo* and in culture. Fibronectin has been shown to also play a role in cellular morphology, cytoskeletal organization, embryonic differentiation and wound repair. Fibronectin is produced by a variety of epithelial and mesenchymal tissues, including the kidney. Vimentin is one of the five major groups of intermediate filaments that are a distinct class of heterogenous cytoskeletal filaments. Vimentin was found to be important for stabilizing the cytoplasm and its behaviour may differ in pathologic conditions. The principle marker of epithelial transformation and fibrosis is α-actin. The relative proportion of actin isoforms differs between organs and changes during development, pathological situations and different culture conditions. Table 2 lists several models of EMT in the kidney.

TABLE 2: Models of EMT in kidney

kidney region & diseased state	**Fibrotic response & details**
Renal Proximal tubule cells	EGF & TGF-β synergistically stimulate proximal tubular cell migration through increased MMP-9 function and enhanced ERK1/2 activation (Tian, Chen et al. 2007)
Distal Tubule (MDCK cells)	HGF induced partial EMT and formation of monoclonal cysts in three-dimensional collagen. (Schramek, Feifel et al. 2003)
Glomerulus	EMT was reversed by early, but not late intervention TGF-β exposure progressively downregulates EGF receptor (Sam, Wanna et al. 2006)
Podocyte	TGF-β resulted in Snail induction which suppressed P-cadherin and nephrin

	In vivo, loss of nephrin and ZO-1 In diabetic nephropathy; desmin, fibroblast specific protein, and MMP9 observed (Li, Kang et al. 2008)
Tubular interstitium Glomerulonephritis	Immunohistochemistry showed expression of α-SMA, & vimentin Loss of epithelial markers directly correlated to grade of tubulo-interstitial disease (Aresu, Rastaldi et al. 2007)
Urinary tract & Collecting duct Unilateral Ureteric Obstruction (UUO)	Obstruction results in cystic dysplasia with loss of the epithelial phenotype and gain of a mesenchymal phenotype Changes associated with disruption of epithelial basement membrane and migration of transitioning cells (Butt, Tarantal et al. 2007)
Collecting duct epithelial cells (IMCD-3)	IGF induced Akt and GSK-3B phosphorylation leading to disruption of E-cadherin-β-catenin complex TGF-B induced activation of Smad3 & ERK1/2 Phenotypic transformation to a mesenchymal morphology Increase in vimentin and α-SMA and decrease in E-cadherin detected as early as 24 hours after stimulation (Ivanova, Butt et al. 2008)

1.3.4 PPARγ, E-cadherin, and β-catenin

E-cadherin is a Ca^{2+}-dependent cell adhesion molecule that plays an important role in the development and maintenance of renal epithelial polarity. E-cadherin is abundant in the distal tubule, collecting duct and most medullary segments, but present at low levels in the proximal tubule (Prozialeck, Lamar et al. 2004). E-cadherin is an integral, transmembrane protein that is generally localized at the adherens junctions of epithelial cells. The extracellular domain of the cadherin contains the Ca^{2+} binding sites, as well as the adhesive regions of the molecule. The intracellular domain is bound to β-catenin

that is bound to α-catenin, which in turn links the entire complex to the actin cytoskeleton. Catenin-cadherin binding is considered to be of high affinity generally as the binding domains span a large surface area of approximately 6100 $Å^2$. The phosphorylation of E-cadherin may increase its binding affinity for β-catenin, which may in turn regulate the behaviour of cadherin-mediated adhesion and the availability of cytoplasmic β-catenin. The differential renal expression and localization of cadherins raises the argument that this disparity may contribute to the differences in the susceptibility of various nephron segments to renal pathology or nephrotoxic injury.

β-catenin also functions as a component of the Wnt nuclear signalling pathway activating the transcription of critical target genes responsible for cellular proliferation and differentiation (Surendran, McCaul et al. 2002). β-catenin acts as a co-activator of T-cell factor (TCF)/ lymphocyte enhancer factor (LEF) transcription factors (Liu, Wang et al. 2006). In the absence of the Wnt signal, β-catenin exists within a cytoplasmic degradation complex which includes β-catenin / glycogen synthase kinase 3β (GSK3β) / adenomatous polyposis coli (APC)/ axin. Induction of β-catenin proteasomal degradation depends on N-terminal phosphorylation by GSK3β. Binding of Wnt glycoproteins to the Frizzled family of receptors results in the inactivation of GSK3β, thereby enhancing the stability of β-catenin leading to the accumulation of unphosphorylated β-catenin capable of nuclear translocation subsequent LEF/TCF transcriptional activity. Two APC-dependent proteasomal degradation pathways have been suggested to degrade excess β-catenin in normal cells, one involving GSK3β and the other involving p53-Siah-1 (Sharma, Pradeep et al. 2004).

TGF-β signalling and its downstream effectors (Smads) have been shown to increase in a co-ordinated fashion with Wnt pathways in the

nucleus (Kispert, Vainio et al. 1998). The Wnt pathway in this case may be regulated by the availability of β-catenin signalling through the disruption of the cadherin-catenin complex or by the repression of cadherin expression (Nelson and Nusse 2004). The co-localization of the TGF-β_1 type II receptor with the β-catenin adherens junction complex has been linked with the generation of a stabilized form of β-catenin that becomes associated with the TGF-β_1-signalling molecule Smad4. This co-operative TGF-β_1 and Wnt signalling has been shown in renal proximal tubular epithelial cells (Tian and Phillips 2002). Mapping of the LEF1 protein-protein domains indicate that β-catenin and Smad3 are capable of binding to different regions on LEF1. The distinct binding sites for β-catenin and Smads suggest a mechanism for the synergistic activation of the TGF-β_1 and Wnt pathways (Labbe, Letamendia et al. 2000).

Expression of E-cadherin has been shown to vary inversely with vimentin and Fibronectin in several diseased states. Elevated vimentin expression was strongly correlated with reduced proliferation indices, active Wnt signalling, and TGF-β signalling, as demonstrated by its dependence on Smad3. The WNT-dependent features of EMT have been termed "truncated EMT". These unexpected observations are interpreted as reflecting the involvement of a core of the EMT system during the tissue remodeling of early tumorigenesis (Chen, Halberg et al. 2008). Fibronectin has also been shown to involve some elements of the WNT pathway as β-catenin was shown to stimulate Fibronectin gene transcription (Gradl, Kuhl et al. 1999) as well as a Wnt-4 expressing myofibroblasts producing higher levels of Fibronectin in a unilateral ureteral obstruction (UUO) (Surendran, McCaul et al. 2002).

PPARγ has been shown to interact with members of the cadherin-catenin cytoskeletal complex through the functional PPRE described in E-cadherin (Annicotte, Iankova et al. 2006), as well as its catenin

binding domain (CBD) which interacts directly with the TEC/LCF domain in β-catenin (Liu, Wang et al. 2006). Nonetheless, studies have also shown that PPARγ activation can induce the proteasomal degradation of β-catenin as well as a reduction in E-cadherin in several cell types, including hepatocytes (Sharma, Pradeep et al. 2004). In normal cells, PPARγ can function to suppress Wnt signalling by targeting phosphorylated β-catenin to the proteasome through a process involving the abovementioned catenin binding domain (Chou, Wang et al. 2007). PPARγ reciprocates with Wnt to dictate events that lead to either growth or differentiation of adipocytes. Potent ligands such as TZDs can relieve Wnt inhibition allowing for differentiation of adipocytes while also inhibiting growth via activation of PPARγ and its transcription factor partner, C/EBPb (Mulholland, Dedhar et al. 2005). Table 3 lists studies where interactions between PPARγ and pro-fibrotic cytokines are described.

TABLE 3: PPARγ and Fibrosis

Fibrotic / Disease Model	**Results, Details, & Mechanism**
Pulmonary fibrosis	Characterized by excessive ECM accumulation and anatomic remodeling Lung (myo)fibroblast treatment with PPARγ agonists resulted in inhibition of proliferative responses, induced cell cycle arrest and inhibited collagen secretion (Milam, Keshamouni et al. 2008)
DOCA-salt rat model of cardiac fibrosis through hypertension	PPARα & γ agonists prevented cardiac fibrosis and the increase in ET-1 mRNA content (Iglarz, Touyz et al. 2003)
Cystic fibrosis of airway epithelium	Inhibition of NFκB by PPARγ agonists reduced airway inflammation in response to acute infection (Perez, van Heeckeren et al. 2008)
TGF-β mediated	Troglitazone inhibited TGF-β_2-induced collagen I

fibrogenesis in retinal pigment epithelial cells	and Fibronectin Troglitazone inhibited TGF β_2-induced Smad2 and Smad3 phosphorylation. (Cheng, Ho et al. 2008)
Cultured mesangial cells exposed to TGF-β	PPAR-gamma agonists induced HGF expression (Li, Wen et al. 2006) Incubation with PGJ_2, TRO and ciglitazone suppressed TGF-B_1-mediated α-SMA, Fibronectin, and PAI-1 expression. (Guo, Koya et al. 2004)
Renal fibrotic lesions in diabetic nephropathy & nondiabetic chronic kidney diseases	PPARγ agonists inhibited TGF-β induced renal fibroblast activation, CTGF expression and ECM synthesis through abrogating of the TGF-β/Smads signalling pathway. (Wang, Liu et al. 2007)
Db/db mice	Tesaglitazar treatment abolished high glucose-induced collagen production, improved insulin resistance, glycemic control, lipid profile and attenuated albuminuria and renal glomerular fibrosis. (Cha, Zhang et al. 2007)
Proximal tubule cells exposed to high glucose	PPARγ agonists exert antifibrotic effects in high glucose by attenuating the increase in AP-1, TGF-β, and Fibronectin. (Panchapakesan, Sumual et al. 2005) PPARγ interacted with HGF (Li, Wen et al. 2006)
Human cortical fibroblasts	Pioglitazone causes an antiproliferative effect and reduces ECM production by reducing TIMP activity, independent of TGF-β (Zafiriou, Stanners et al. 2005)
Glomeruli from streptozotocin-induced diabetic rats & glomerular sclerosis	Troglitazone reduced expression of ECM proteins and TGF-β PPAR-γ agonists ameliorate the progression of glomerulosclerosis. (Izzedine, Launay-Vacher et al. 2005)
Insulin-dependent diabetes mellitus & insulin sensitive PPARγ deficient mice	TZDs had an anti-proteinuric, hemodynamic, and antihypertensive effects TZDs shown to lower blood pressure in diabetic patients with hypertension and patients with diabetic nephropathy through multiple mechanisms (Izzedine, Launay-Vacher et al. 2005) Mice were protected against renal injury and systemic metabolic abnormalities associated with consumption of a high fat diet (Kume, Uzu et al. 2007)
Peritoneal fibrosis	TRO reduced the expression of profibrotic, inflammatory cytokines, and growth factors as well as components of the ECM (Fibronectin and

	type IV collagen) (Peng, Liu et al. 2006)

1.4 Rationale

The collecting duct has only recently been identified as a contributor to interstitial fibrosis however the full fibrotic response of the CD *in vitro & in* vivo requires clarification. There have been several studies in a unilateral ureteral obstruction model which involves the blockage of the ureteral tract and an evident fibrotic response. A fetal urinary tract obstruction model resulted in a collecting duct epithelial to mesenchymal transition, contributing to the interstitial changes associated with poor prognosis (Butt, Tarantal et al. 2007). Only recently has the same group characterized *in vitro* an EMT event in a collecting duct cell line (Ivanova, Butt et al. 2008). The difficulty with the collecting duct however, is that it spans from the cortex to the outer and inner medulla. These three regions differ greatly and their environments affect the cellular behavior. The IMCD-3 cell line, representing the terminal section of the inner medulla has been shown to undergo EMT upon TGF-β & IGF stimulation (Ivanova, Butt et al. 2008). The other two isolated cell lines, IMCD-K2 and M1, have yet to be characterized in response to TGF-β and other pro-fibrotic cytokines. Because PPARγ agonists are becoming more popular and have shown protective effects in other segments of the nephron, Troglitazone's effect on collecting duct fibrosis was examined.

1.4.1 Purpose

The purpose of this study is to assess the effects of Troglitazone on EMT in the collecting duct cell lines M1 & IMCD-K2.

1.4.2 Hypothesis

TGF-β will initiate an epithelial to mesenchymal transformation in the collecting duct epithelial cell lines IMCD-K2 and M1 which will be attenuated by Troglitazone.

1.4.3 Objectives

1) To induce a mesenchymal transformation in M1 & IMCD-K2 cells.

Light microscopy was used to identify any morphological changes in reponse to TGF-β and EGF stimulation. The morphological changes expected include a loss of cell-to-cell contact which promotes a more mobile phenotype generally observed in metastatic tissue. The expression of profibrotic markers were examined through Western Blot and immunofluorescence.

2) To examine whether Troglitazone, a synthetic PPARγ ligand promotes or inhibits a fibrotic response in M1 & IMCD-K2 cells.

The expression levels of epithelial & mesenchymal markers were quantified by Western Blot upon exposure to Troglitazone. Morphological changes were examined through light and fluorescent microscopy.

3) To verify whether the effects of Troglitazone were PPARγ-dependent.

GW9662 & T0070907 were used as *PPARγ* antagonists in conjunction with Trolgitazone. PPARγ was also over-expressed in M1 cells through transient

transfection. PGJ_2 was also used as a comparison, being a non-TZD endogenous PPARγ ligand.

2.0 METHODS

2.1 Cell Culture

2.1.1. Inner medullary collecting duct cell line (IMCD-K2):

The IMCD handles the final phase of urine concentration through sodium and water exchange. It maintains homeostasis depending on dietary intake through intercalated cells which regulate pH, bicarbonate (HCO_3^-) reabsorbtion and secretion of H^+. The inner collecting duct functions in a hypoxic and harsh environment. Its ability to survive and function efficiently under these conditions makes it an interesting model to study fibrosis.

The IMCD-K2 cell line was originally isolated and characterized by Dr. Bruce Stanton (*Dartmouth Medical School*). IMCD-K2 cells were grown in DMEM:F-12 (1:1) media supplemented with 10% FBS, 1% Insulin-Transferrin-Selenium, 1% Penicillin-Streptomycin, 1% L-glutamine and 5μM dexamethasone and were maintained at 5% CO_2 and 37°C during culture and treatment. The IMCD-K2 cell line is derived from the initial section of the kidney's inner medullary collecting duct. These cells are commonly used in electrochemical potential, ion retention, and sodium transport studies. Overall, *in vitro* experiments have shown high behavioural correlation with the *in vivo* CD (Kizer, Lewis et al. 1995).

2.1.2. Cortical collecting duct cell line (M1):

The M1 mouse cortical collecting duct cell line is a heterogeneous population of principal, α-, and β-intercalated cells; derived from the cortical collecting duct of an SV40 transgenic mouse. These cells have been shown to possess the characteristics of the *in vivo* CCD, both in terms of morphology and physiological properties (Stoos, Naray-Fejes-Toth et al. 1991). M-1 mouse cortical collecting

duct cells *(ATCC # CRL-2038)* were grown at 37°C and 5% CO_2. The culture media consisted of DMEM:F-12 media (1:1), pH 7.4, containing 5% FBS and 1% Pen-Strep.

2.1.3. Proximal Tubule (MCT):

MCT renal proximal tubule cells were a gift from Dr. David Plieth (*VanderBilt University School of Medicine*), they were cultured in DMEM:F-12 (1:1) supplemented with 10% FBS and 1% Pen-Strep and were maintained at 5% CO_2 and 37°C during culture and treatment. The MCT cell line was derived from proximal tubular epithelial cells from mice which developed autoimmune interstitial nephritis. MCT cells were originally isolated to be used as a model of a nephritogenic immune response, and as a potential source for new extracellular matrix which develops as a fibrogenic response to interstitial nephritis (Haverty, Kelly et al. 1988).

2.2 Ligands, antagonists, growth factors, and GSK-3β inhibitor

Troglitazone (Sigma) was the primary TZD used and the majority of the experiments pertain to the effects of Troglitazone in the collecting duct. The PPARγ antagonist GW9662 (Cayman Chemicals) is an irreversible antagonist that binds PPARγ with an IC50 in the nanomolar range, and is 10- and 600-fold less potent in binding PPARα and PPARδ, respectively. T0070907 has also been identified as a potent and selective PPARγ antagonist with an apparent binding affinity of 1 nM. T0070907 covalently modifies cysteine 313 in helix 3 of PPARγ and affects the conformation of helix 12 in the ligand binding domain, modulating PPARγ cofactor recruitment. Both antagonists were used alongside Troglitazone.

To evaluate the effects of TGF-β (R&D systems), EGF (Sigma), Troglitazone (Sigma), PGJ_2 (Cayman Chemical), GW9662 (Cayman Chemical),

and T0070907 (Cayman Chemical), sub-confluent 100mm plates were starved for 24 hours by replacing the culture media containing serum with DMEM:F-12 (1:1). Troglitazone, GW9662, T0070907, GW501516 and PGJ_2 were dissolved in DMSO to their suggested concentrations (20ng/mL - 50ng/mL). Recombinant TGF-β was reconstituted in a saline solution to a stock concentration of 4mg/mL. The treatment concentration ranges were between 1μM and 10μM for Troglitazone, T0070907, GW9662; 1ng/mL to 20ng/mL for TGF-β and EGF; and 10^{-9}M to 10^{-5}M for PGJ_2.

SB216763 (Sigma) is a structurally distinct maleimide that inhibits GSK-3β *in vitro* in an ATP competitive manner with an IC_{50} value of 34 nM. SB216763 has been shown to increase levels of β-catenin and is used in cancer and cardiovascular research. LiCl has also been shown to inhibit GSK-3β function. This inhibition of GSK-3β is currently believed to underlie the therapeutic usefulness of lithium salts for the treatment of mood disorders. To evaluate whether SB216763 or LiCl (Sigma) could reverse the effect of Troglitazone on β-catenin, sub-confluent 100mm plates were starved for 24 hours by replacing the culture media with serum-free DMEM:F-12 (1:1). SB216763 was dissolved in DMSO to a stock concentration of 50mM. LiCl was dissolved in dH_2O at 2.5M and sterilized by filtration. Cells were co-treated with 2.5μM and 5μM Troglitazone and 10uM SB-216763. M1 cells were also treated with 25μM & 50μM LiCl.

2.3 Western Blot

Time courses were performed from 24 hours to 96 hours for Troglitazone and TGF-β in order to determine the ideal time point for further experiments. Following stimulation, total protein isolation was performed using RIPA lysis buffer. Briefly, the media was removed and plates were washed with ice cold PBS. Cells were collected using cell

lifters in 1mL PBS and spun at 2000 *x* g for 10 minutes. The supernatant was discarded and the cell pellets were re-suspended in protein lysis buffer consisting of RIPA buffer [1% Nonidet P-40, 1% sodium deoxycholate, 0.1% sodium dodecyl sulphate (SDS, w/v), 4.5 mM NaCl, 2.5 mM Tris (pH 7.4), 8 µM EDTA, 0.2 mM sodium phosphate (pH 7.2)], 10mM sodium fluoride, 1mM sodium pyrophosphate, 100 µM sodium orthovanadate, 1:100 protease inhibitor cocktail (Sigma) and 500µM PMSF. The solution was centrifuged at 10,000 *x* g for 10 minutes and the supernatant was transferred to a clean eppendorf tube.

Protein was quantified by spectrophotometry using Bradford reagent, and denatured by boiling the samples at 95°C for 5-10 minutes. The samples were briefly centrifuged, placed on ice, and equal amounts of protein (generally 15µg to 50µg) were loaded on a 10% acrylamide resolving gel with a 4% stacking gel. Electrophoresis was performed at 180V for approximately 60 minutes. Protein was transferred onto a nitrocellulose membrane (Amersham) at 100V for 75 minutes. The nitrocellulose membrane was blocked in 10% milk in TBS/T for 1 to 3 hours and a primary antibody was applied directly to the milk and left overnight. Three 20 minute washes were performed after the primary antibody solution was removed and the appropriate secondary antibody was applied in 10% milk-TBS/T for 90 minutes, after which the membrane was washed with TBS/T five times. The HRP conjugated secondary antibodies were developed with Pierce SuperSignal® chemiluminescent reagent for 5 minutes and exposed to Kodak X-Omat™ Blue XB-1 film as well as digitally exposed using the Alpha Innotech FluorchemHD2 imaging system. A list of primary and secondary antibodies used is provided in Table 4.

TABLE 4: Immunoblotting Antibody Conditions

1° Antibody	Dilution (μL)	2° Antibody	Dilution (μL)	Protein (μg)
α-sma (Sigma)	1:1000	α-mouse HRP (Promega)	1:2000	≥50
β-actin (Sigma)	1:10000	α-mouse	1:4000	10-100
α-catenin (Sigma)	1:4000	α-rabbit	1:4000	20
β-catenin (R&D System)	1:2000	α-mouse	1:2000	50
β-catenin (Sigma)	1:4000	α-rabbit	1:4000	20
E-cadherin (Sigma)	1:4000	α-rat HRP (R&D Systems)	1:5000	20
Fibronectin (Sigma)	1:5000	α-rabbit	1:4000	20
PPARγ (Santa Cruz Biotech)	1:400 - 1:2000	α-mouse	1:2000	≥50
p-ERK 1/2*	1:1000	α-rabbit	1:2000	20
Total-ERK 1/2*	1:1000	α-rabbit	1:2000	20
p-JNK*	1:1000	α-rabbit	1:2000	20
Total JNK*	1:1000	α-rabbit	1:2000	20
p-p38*	1:1000	α-rabbit	1:2000	20
Total p38*	1:1000	α-rabbit	1:2000	20
Total smad 2/3	1:1000	α-goat	1:2000	20-50
Vimentin (Sigma)	1:1000	α-mouse	1:2000	≥50
MMP-2 (Santa Cruz Biotech)	1:400 - 1:2000	α-mouse	1:2000	≥50
MMP-9 (Santa Cruz Biotech)	1:400 - 1:2000	α-mouse	1:2000	≥50
N-cadherin (Sigma)	1:1000	α-mouse	1:2000	≥50

* = 5% BSA in TBS-T as opposed to 10% milk in TBS-T

2.4 Immunofluorescence

Cells were plated on cover slips in 6 well plates and allowed to adhere overnight. The cells were starved for 24 hours to remove additional growth factors and stimulated with Troglitazone, GW9662 and TGF-β. Once apparent morphological changes were observed (24 hours - 96 hours) the plates were removed from incubation. The media was replenished every two to three days. The cover-slips were washed with PBS to remove traces of media, and fixed for 30 minutes at room

temperature (RT) in 4% paraformaldehyde (PFA) or at -20°C in a 1:1 Methanol-Acetone solution. Excess fixative was washed with PBS/Mg^{2+}/Ca^{2+} for 2 x 5 minutes. 0.1% Triton-X in PBS was used for permeabilization for 30 minutes at room temperature followed by 3 x 5 minute washes in PBS/Mg^{2+}/Ca^{2+}. The cover slips were blocked in 1% BSA in 0.1% Triton-X in PBS/Mg^{2+}/Ca^{2+} for 30 minutes prior to adding the antibody of choice. All antibodies were diluted in 1% BSA in 0.1% Triton-X in PBS/Mg^{2+}/Ca^{2+}. Cells were incubated with anti-smooth muscle actin (Sigma) and placed O/N at 4°C as well as Phalloidin-FITC for 1 hour at RT in the dark. 3 x 5 minute PBS/Mg^{2+}/Ca^{2+} washes were performed prior to the addition of the secondary antibody, α-mouse FITC (Sigma) 1:300 for 90 minutes or DAPI (1:1000) for 15 minutes. 3 x 5 minute washes were performed prior to mounting the coverslips in Fluoromount G mounting media (Southern Biotech, cat. #17984-25). The edges of the coverslips were sealed with nail polish and stored protected from light at 4°C. Images were captured using the Zeiss AxioCam of an Axioskop2 MOT Fluorescent microscope. The primary and secondary antibodies used are listed in Table 5.

TABLE 5: Immunofluorescence Antibody Conditions

1° Antibody	2° Antibody	Conjugate (λ)
α-sma (Sigma)	α-mouse	FITC (490nm), Cy3 (550nm)
AlexaFluor Phalloidin	-	488nm - FITC
α-catenin (Sigma)	α-rabbit	FITC (490nm), Cy3 (550nm)
DAPI	-	365nm
β-catenin (Sigma)	α-rabbit	FITC (490nm), Cy3 (550nm)
E-cadherin (Sigma)	α-rat	FITC (490nm)
Fibronectin (Sigma)	α-rabbit	FITC (490nm), Cy3 (550nm)
AQP-2	α -goat	Cy3 (550nm)
Pan-cytokeratin (Sigma)	α-mouse	FITC (490nm)
Vimentin	α-mouse	FITC (490nm)

2.5 Reverse Transcriptase-PCR for PPARγ

RNA was isolated from confluent IMCD-K2 and M-1 cells using 1mL of TRIzol reagent (Gibco) according to the manufacturer's instructions and was dissolved in 20 μL of diethylpyrocarbonate (DEPC)-treated water. The isolated RNA was then treated with 0.3 U/μg of DNase I (Invitrogen) to remove genomic DNA. The RNA was reverse-transcribed using MuLV (recombinant Moloney murine leukemia virus) reverse transcriptase and random hexamers from the GeneAmp RNA PCR Core Kit (Applied Biosystems) as per the manufacturer's instructions. The cDNA was then amplified using AmpliTaq DNA polymerase and PPARγ primers. The PCR parameters used were 40 cycles of: 95°C for 30 seconds, 59°C for 45 seconds and 72°C for 60 seconds, followed by a final 10 minutes at 72°C. The amplification was carried out using the GeneAMP PCR System 2400 (Applied Biosystems). The PCR products were run on a 1% agarose gel and the bands were visualized using ethidium bromide under UV light with an Alpha Innotech Alpha Imager.

2.6 PPRE-Luciferase Assay

Cells were seeded at densities of 1000 cells/cm^3 in 6-well plates and then transiently transfected with the firefly luciferase vector containing a PPAR response element (PPRE) using Polyfect reagent (QIAGEN, CA, USA) according to the manufacturer's instruction. The PPRE-Luc vector was a gift from Dr. Jasmin (University of Ottawa) and is distributed by Addgene (Plasmid 1015: PPRE X3-TK-luc). The cells were cotransfected with a renilla luciferase PHAG-TK vector to assess transfection efficiency. The renilla PHAG-TK vector was also a gift from Dr. Jasmin (University of Ottawa). Cells were treated for 24 hours with PPARγ ligands, after which a passive lysis buffer was used to quantify firefly and renilla luciferase activities. Activity was measured using the Dual-luciferase

Reporter Assay System (Promega) with a Berthold Lumat LB9507 luminometer. To correct for differences in transfection efficiency, firefly luciferase units were normalized for renilla luciferase activity in each sample.

2.7 PPARγ overexpression

pcDNA, pcDNA-PPARγ, and pcDNA-PPARγ EQ4994 vectors were obtained from Addgene as bacterial stabs. The sizes of each insert were verified with XhoI/HindIII digests. M1 cells were grown to 25% confluence prior to transfection. 4μg of plasmid DNA was diluted to a volume of 150μL in DMEM and 15μL of Polyfect Transfection Reagent (Qiagen) was added to the solution. The suspension was then incubated at room temperature for 10 minutes, mixed with 1mL of culture media containing 0.1% ampicillin and added to the culture plate. This was repeated 48 hours later for the final 24 hours of the 72 hours transfection period.

2.8 Restriction digest

The reaction tubes were prepared containing the following reagents; dH_2O, 10X restriction enzyme (RE) buffer, plasmid DNA, Xho1, and HindIII. It should be noted the restriction enzymes were not removed from storage and where kept on ice until the moment they were required to preserve their function. The contents were mixed gently and placed in a microcentrifuge for a few seconds. The reactions were incubated at 37°C for an hour. 5-10μL of digested sample was removed, added to DNA loading buffer and separated by electrophoresis on a 1% agarose gel. The bands were visualized with an Alpha Innotec Alpha Imager under the ethidium bromide filter.

2.9 DCFDA ROS Assay

Cells were plated in a 6 well culture dish and allowed to reach 60-70% confluence prior to 24 hour stimulation with 2.5μM & 5μM TRO, as well as 0.5μM PGJ_2, alongside 10μM GW9662 co-treatment. After 24 hours of stimulation, the cells were removed from incubation. The media was removed and the cells were washed with PBS and then trypsinized. Once detached, the trypsin was neutralized using a 10% FBS-PBS solution and the cells were centrifuged. A 10mM stock solution of DCFDA (2´-7´-dichlorofluorescin diacetate) was diluted in PBS to 2μM and the pellet was resuspended and incubated in the 150μL of the DCFDA-PBS solution for 30 minutes. The following steps were performed under minimal light as the product of DCFDA and H_2O_2 is light sensitive. The samples were then centrifuged and resuspended in 150μL PBS. Fluorescence was read using a Varian Cary Eclipse fluorescence spectrophotometer with excitation and emission wavelengths of 485nm and 535nm respectively. The cell number was determined using a Beckman Coulter particle counter. Fluorescence was then normalized to cell number and analyzed.

2.10 Statistics

GraphPad Prism v4.03 was used to plot and analyse the data collected. Values are expressed as means ± standard error of the mean (S.E.M.). An unpaired t-test was used to assess statistical significance between selected experimental groups. A one-sample t test was performed against a hypothetical value of 1.0 for all groups as the values represented fold controls where the control groups all had values of 1.0. A p-value $\leq$ 0.05 was regarded as statistically significant.

3.0 RESULTS

3.1 EMT in the collecting duct cell lines IMCD-K2 & M1

IMCD-K2 & M1 collecting duct cells were stimulated with TGF-β and the potential transformation of these epithelial cell lines were assessed by light microscopy and Western blot. Cell-to-cell contact is disrupted in the transformation of epithelial cells, leading to morphological changes. These morphological changes were assessed through light microscopy. There was no evident disruption in IMCD-K2 & M1 cell-to-cell contact upon 24 hour to 96 hour TGF-β stimulation, as they were able to reach confluence (Fig. 3a). No increase in α-SMA (Fig. 3b) or decrease in E-cadherin (Fig. 3c) was observed in the TGF-β treated IMCD-K2 cells.

The levels of α-SMA in M1 cells did not increase upon treatment with 4ng/mL TGF-β for 48 hours verified through immunofluorescence (Fig. 4a & 4b). The levels of E-cadherin were also constant after prolonged exposure to TGF-β, showing no signs of a decrease through Western blot (Fig. 4d & 4e). The fact E-cadherin protein levels were not decreased in either collecting duct cell line reflects the overall lack of a response to the cytokine at 2ng/mL to 5ng/mL, and at elevated doses of 10ng/mL and 20ng/mL. In addition, co-stimulation of IMCD-K2 & M1 cells with TGF-β and 20ng/mL EGF, which has been shown to have a synergistic effect with TGF-β, did not result in an increase in α-SMA or decrease in E-cadherin.

The MCT proximal tubule epithelial cells, used as a control to verify the TGF-β integrity, transformed into a spindle-like phenotype after the first 24 hours of treatment at both 1ng/mL and 2ng/mL TGF-β (Fig. 5a). The elongated phenotype was consistent through 48 hour to 72 hour stimulation. TGF-β appeared to cause some cell death and cell

growth arrest in the MCT cells, accounting for the difference in cell numbers between control (Fig 5b) and treated slides (Fig 5c). A 4-fold increase in α-SMA expression was detected in the TGF-β treated MCT cells, as shown through immunofluorescence and Western blotting (Fig. 5d).

The IMCD-K2 & M1 cell lines showed a subpopulation of α-SMA expressing cells when high concentrations of antibody were used and large quantities of protein were examined. This sub-population of α-SMA expressing cells has previously been shown in the collecting duct *in vivo* (Butt, Tarantal et al. 2007). Therefore the detection of α-SMA in these cell lines does not contradict their epithelial nature.

A)

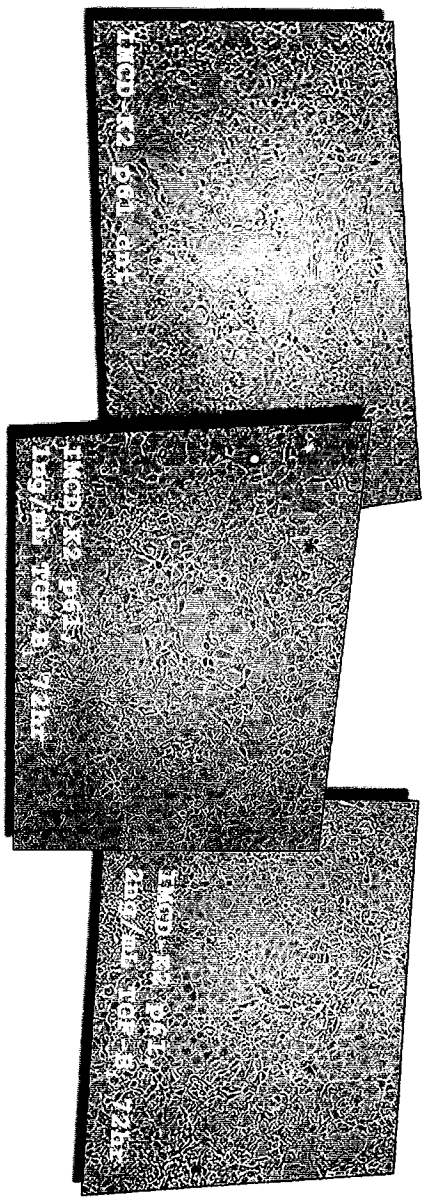

B)

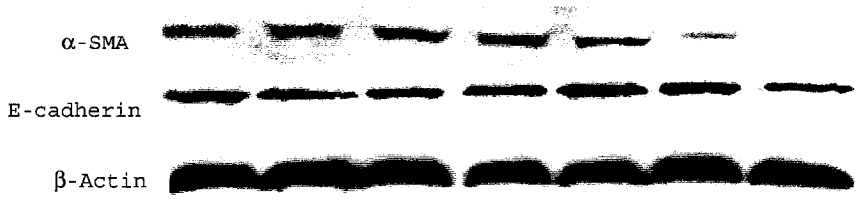

TGF-β (ng/mL)	-	2	5	10	-	2	5
EGF (ng/mL)	-	-	-	-	20	20	20

C)

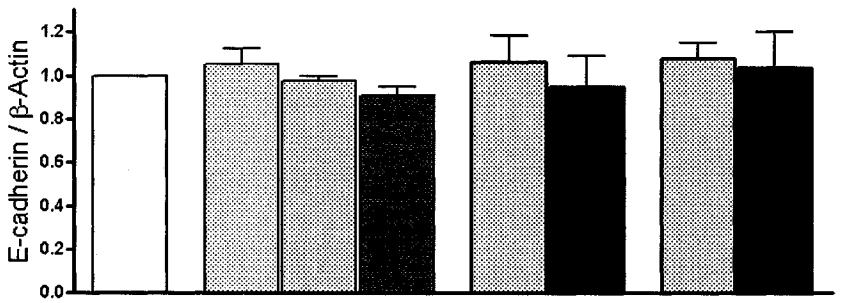

		48 HOUR					96 HOUR	
		(ng/mL)						
TGF-β	-	2	5	10	-	5	5	10
EGF	-	-	-	-	20	20	-	-

Fig. 3 - TGF-β does not induce morphological changes, increase α-SMA or attenuate E-cadherin in IMCD-K2 cells

IMCD-K2 cells were plated on cover-slips in a 6 well plate and stimulated with TGF-β at 1ng/mL and 2ng/mL for 72 hours. Light microscopy was used to verify whether any morphological changes could be observed after 72hr incubation at 100X magnification (A). IMCD-K2 cells were also plated and stimulated with TGF-β at 2ng/mL, 5ng/mL, and 10ng/mL. EGF was used at 20ng/mL alone and concurrently with 5ng/mL of TGF-β for 48 hours. Protein was isolated from IMCD-K2 cells and separated by SDS-PAGE. Western blot was used to analyze E-cadherin and α-SMA (B). The results for E-cadherin were normalized to β-actin (C). Values represent mean ± S.E.M.

A)

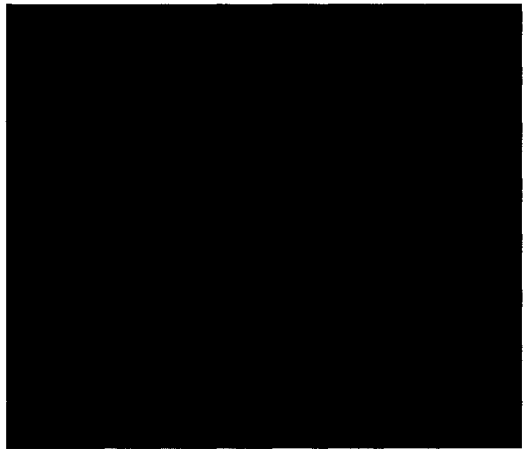

M1 CTL 48HRS

B)

M1 4ng/mL TGF-β 48HRS

C)

VSMC

D)

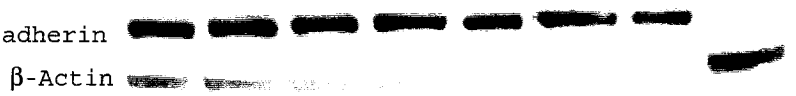

TGF-β	-	10ng/mL	-	5ng/mL	5ng/mL	10ng/mL	10ng/mL	VSMC
EGF	-	-	-	-	20ng/mL	-	20ng/mL	

E)

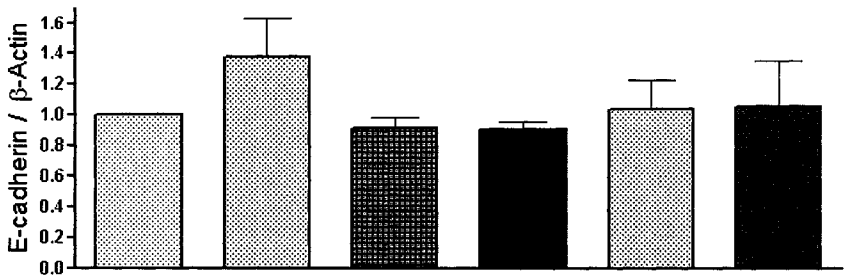

		48 HOURS			96 HOURS	
		ng/mL				
TGF-β	-	4	-	4	10	20
EGF	-	-	20	20	-	-

Fig. 4 - TGF-β does not increase α-SMA or attenuate E-cadherin expression in M1 cortical collecting duct cells

M1 cells were plated on cover-slips in a 6 well plate and stimulated with 4ng/mL TGF-β for 48 hours. Immunofluorescence was used to observe α-SMA expression, visualized by the green FITC signal, in response to treatment at 200X magnification (A, B). Vascular smooth muscle cells (VSMC) were plated and probed with α-SMA as an experimental control (C). M1 cells were also plated and stimulated with TGF-β at 4ng/mL for 48 hours and 10ng/mL and 20ng/mL for 96 hours. E-cadherin levels were determined by Western blot and normalized to β-actin (D, E). Values represent mean ± S.E.M.

A)

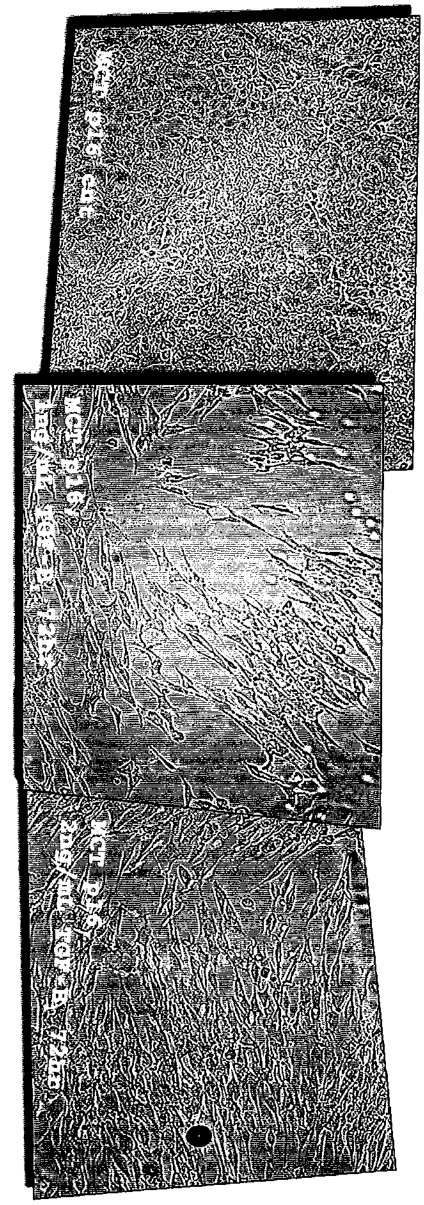

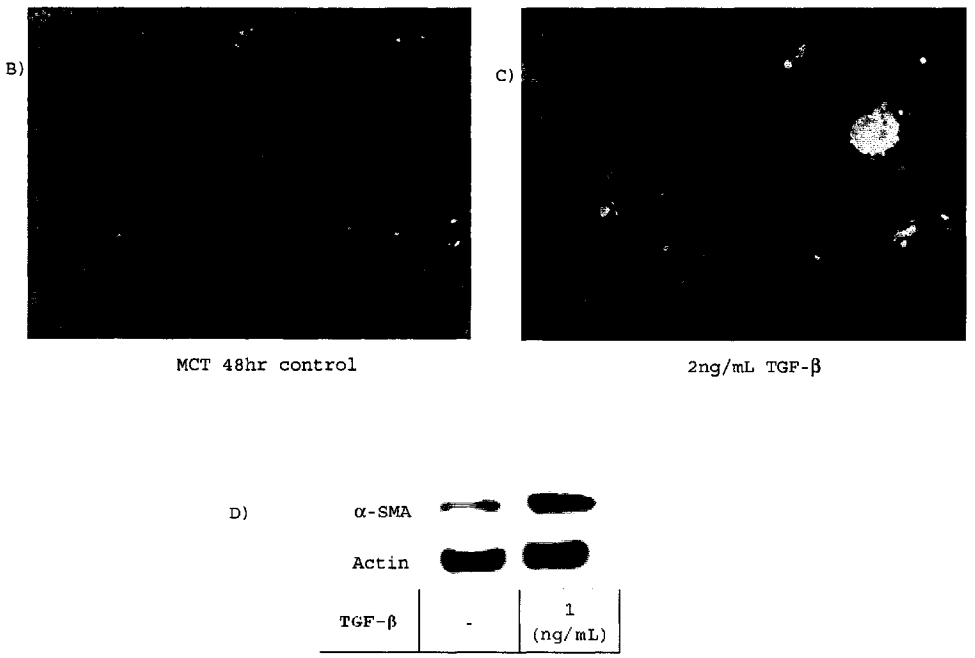

Fig. 5 - TGF-β induces morphological change and increases α-SMA in MCT proximal tubule cells

MCT cells were plated on cover-slips in a 6 well plate and stimulated with TGF-β at 1ng/mL and 2ng/mL for 72 hours. Light microscopy was used to depict the morphological changes observed after 72 hours of incubation (A). Immunofluorescence was also performed on MCT cells treated with 2ng/mL TGF-β for 48 hours, α-SMA was visualized by the green FITC signal with DAPI stained nuclei in blue (B, C) at 100X magnification. Western blotting of 30μg MCT protein was also carried out for α-SMA and β-actin (D).

3.2 Troglitazone induces morphological changes in the IMCD-K2 & M1 collecting duct cell lines

PPARγ is present in both the M1 & IMCD-K2 cell lines (Fig. 6). The general effects of TZDs in the kidney have been protective however the treatment of IMCD-K2 & M1 cells with TRO resulted in a decrease in cell to cell contact, disorganization of the F-actin cytoskeleton filament network, and a less rounded, elongated spindle like shape at 2.5μM & 5μM, visualized through FITC-conjugated Phalloidin (Fig. 7). These morphological changes were not reversed by the PPARγ antagonist GW9662 at 10μM, and in some cases it further disrupted cellular organization, suggesting a PPARγ-independent pathway is in effect.

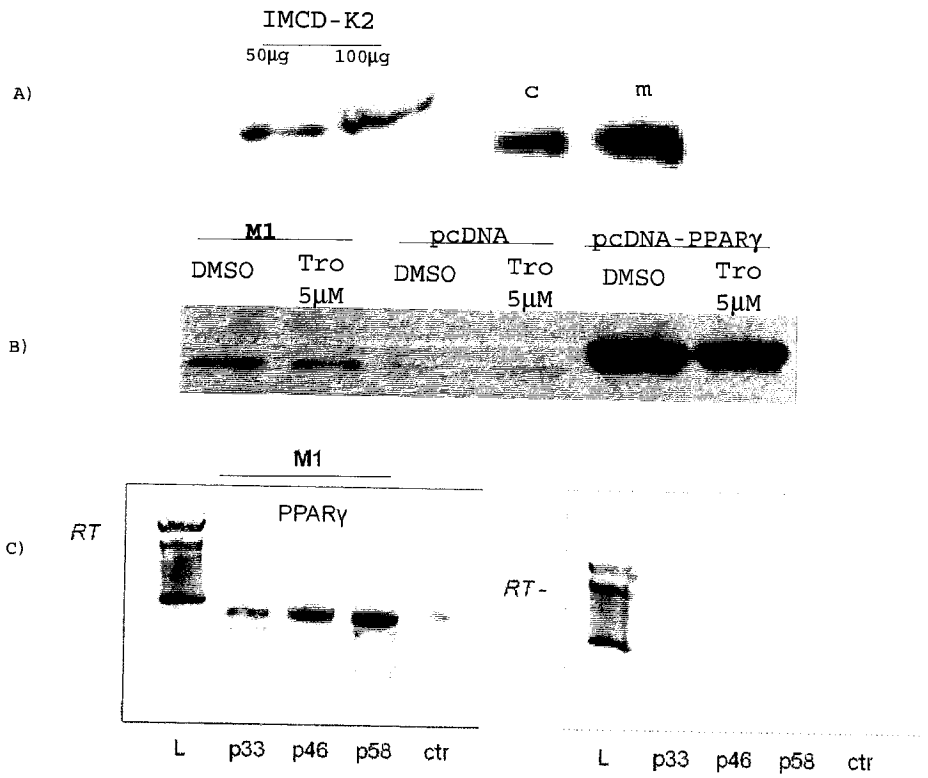

Fig. 6 - PPARγ is present in the IMCD-K2 & M1 collecting duct cell lines To verify the presence of PPARγ in the IMCD-K2 cell line, 50µg and 100µg of protein were separated by SDS-PAGE. An antibody against PPARγ was used to detect a band at 67kDa (A). Mouse cortex (c) and medulla (m) lysate were used as positive controls. In M1 cells, PPARγ was over-expressed through transient transfection with a pcDNA-PPARγ vector. Endogenous PPARγ levels as well as those of the pcDNA plasmid control and pcDNA-PPARγ over-expression samples were determined by Western Blot (B). RT-PCR was performed with M1 RNA (various passages); a 1% agarose gel was used to separate a product size of approximately 400bp (C). The (RT-) samples were used as a negative control to ensure amplification of the appropriate target sequence.

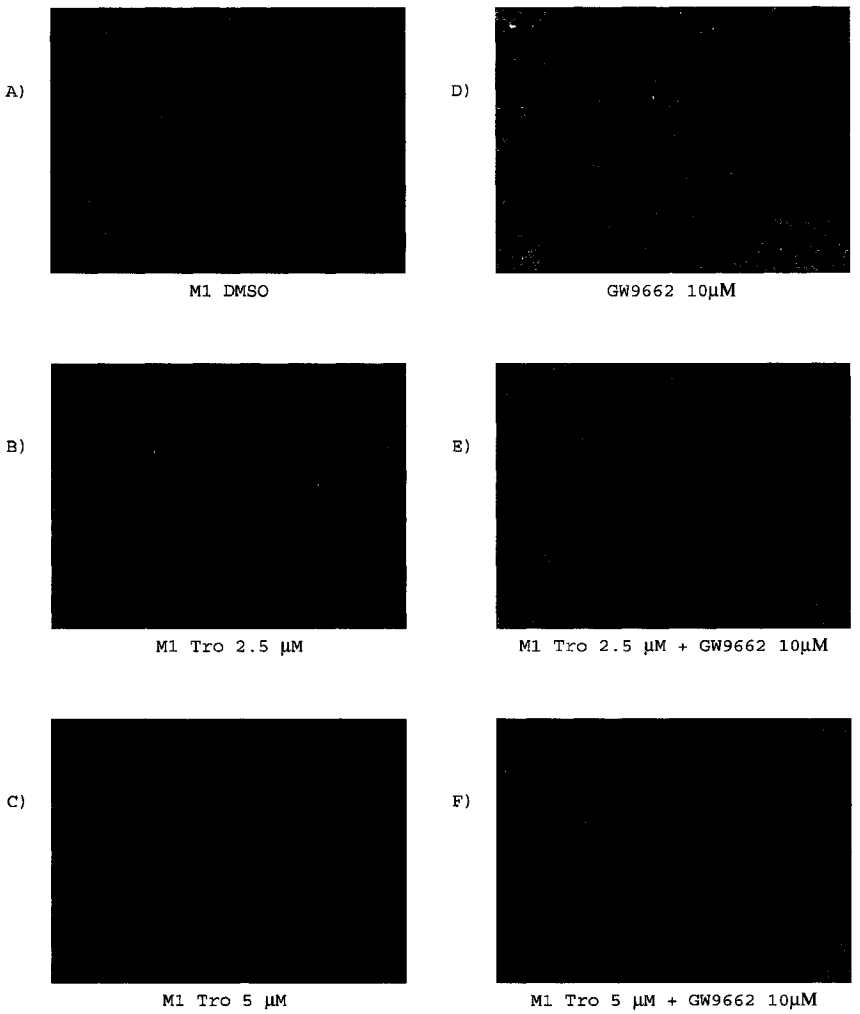

Fig. 7 - TRO induces morphological changes in M1 cells independent of PPARγ

M1 cells were plated on cover-slips in a 6 well plate and stimulated with DMSO, 2.5μM, & 5μM TRO for 24 hours (A, B, C). M1 cells were co-treated with 10μM of GW9662 and with GW9662 alone (E, F, D). The cells were permeabilized with 0.1% Triton-X in PBS and F-actin filaments were stained with FITC-conjugated Phalloidin. A magnification of 100X was used.

3.3 Troglitazone induces cytoskeleton reorganization in the collecting duct cell lines IMCD-K2 & M1

A general characterization of the M1 cell line was performed with immunofluorescence using the markers of interest (E-cadherin, β-catenin, α-catenin, and Fibronectin) as well as Pan-cytokeratin. Aquaporin-2 (AQP-2), specific to the renal collecting duct principal cell (Takata, Tajika et al. 2004), was also used in order to determine that the ratio of intercalated to principal cells was approximately 2:3 (Fig. 8). E-cadherin and β-catenin was present in the cytoplasm as well as at the adhesion points in between cells, in addition to lesser nuclear staining. Fibronectin, which helps form the intracellular cytoskeleton, was located in the cytoplasm with peri-nuclear localization and some nuclear staining. α-catenin demonstrated nuclear and peri-nuclear staining with no staining at adhesion junctions. Pan-cytokeratin stained along the intracellular cytoplasm as well with no nuclear staining.

Along with the aforementioned morphological changes, treatment of IMCD-K2 & M1 cells with TRO resulted in a decrease in several epithelial adhesion markers such as E-cadherin, β-catenin, and α-catenin and an upregulation of Fibronectin. E-cadherin levels were reduced by 50% in both IMCD-K2 and M1 cells at 5μM and by 30% at a concentration of 2μM in M1 cells as early as 24 hours post treatment (Fig. 9). In contrast, PGJ_2 was able to increase E-cadherin levels to 1.5-fold of control (Fig. 10). There were 50% drops in the levels of β-catenin in both IMCD-K2 and M1 cells at 10μM and 5μM respectively, post 24 hours of TRO treatment (Fig. 11). PGJ_2 showed a tendency for an increase in β-catenin in M1 cells (Fig. 12). A 40% reduction was observed in α-catenin levels in M1 cells in response to TRO (Fig. 13).

TRO also caused a near 2-fold increase in Fibronectin in M1 cells at 5μM and showed a strong trend for an increase in IMCD-K2 cells at 10μM (Fig. 14). PGJ_2 showed a tendency for an increase in Fibronectin production in M1 cells (Fig. 15). Despite the trends for a transformation of the epithelial cell lines the negligible increase in α-SMA observed *via* immunofluorescence was not detectable in M1 cells by Western blot (Fig. 16).

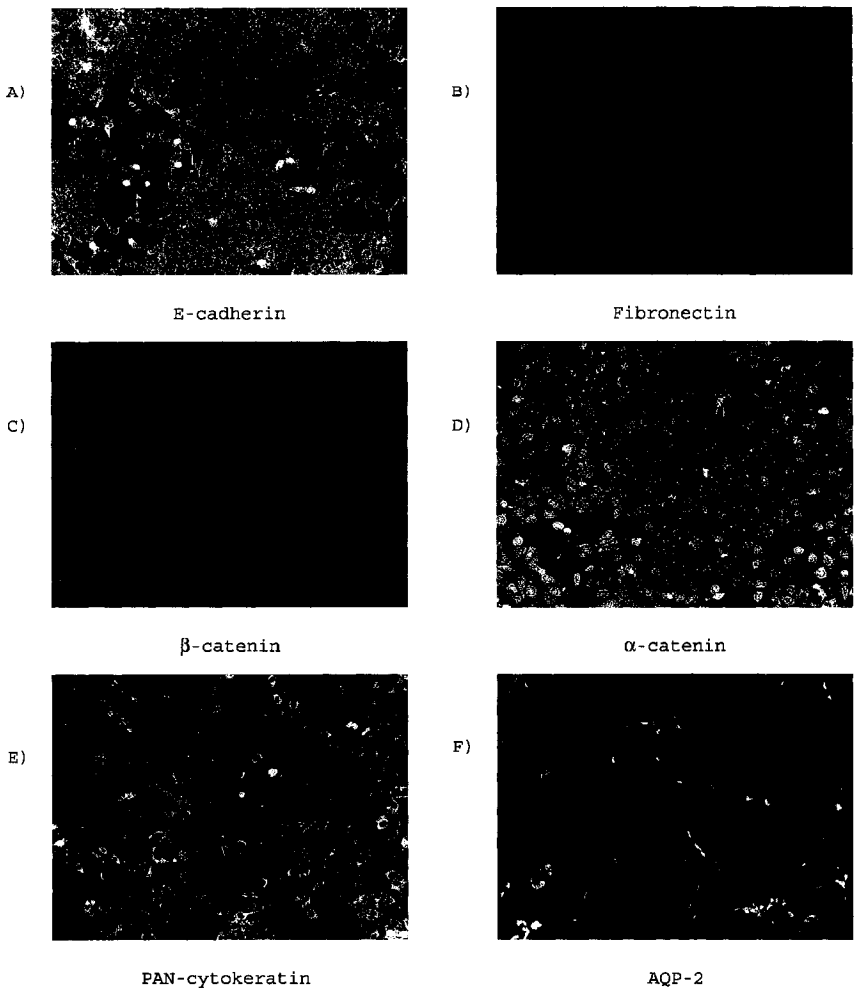

Fig. 8 - Characterization of M1 cells

M1 cells were grown on cover-slips until 80% confluence was reached. The cells were then fixed, permeabilized and blocked with E-cadherin (A), Fibronectin (B), β-catenin (C), α-catenin (D), PAN-cytokeratin (E), and AQP-2 (F) antibodies and fluorescently conjugated anti-rat, mouse, and rabbit secondary antibodies. Immunofluorescence was used to visualize the localization of the various markers at 200X magnification. DAPI (blue) stained nuclei were also visualized for AQP-2 probed cells (F).

A)

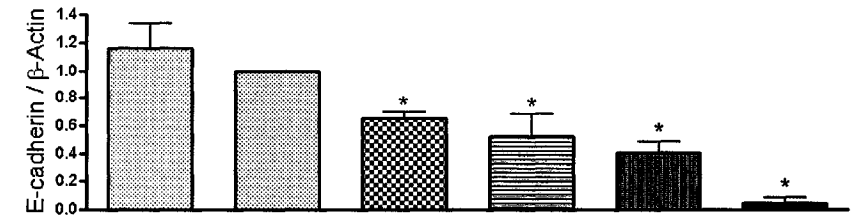

DMSO	-	10µL	-	-	-	-
TRO	-	-	5µM	7.5µM	10µM	25µM

DMSO	-	10µL	50µL		-	-	-
TRO	-	-	-		5µM	7.5µM	10µM

B)

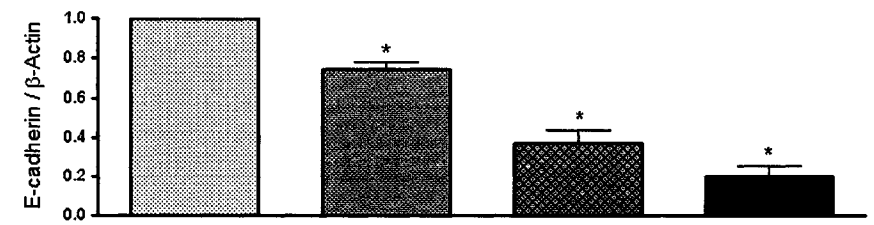

DMSO	10µL	-	-	-
TRO	-	2µM	5µM	7.5µM

DMSO	-	10µL	-	-	-
TRO	-	-	7.5µM	5µM	2.5µM

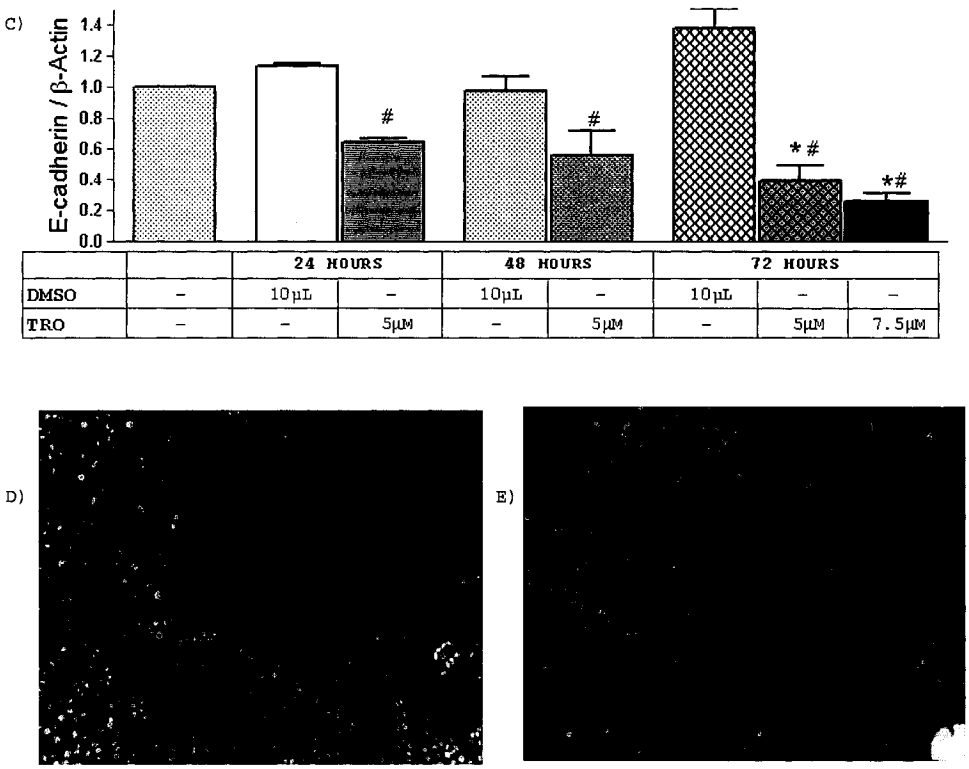

Fig. 9 - TRO attenuates E-cadherin in IMCD-K2 & M1 cells

IMCD-K2 (A) & M1 (B & C) cells were treated with varying concentrations of TRO after 24, 48, and 72 hour starvation. Western blotting was performed on 20μg of protein for E-cadherin and the result was normalized to β-actin, a band size of 120 kDa was obtained for E-cadherin. M1 cells were also grown on cover-slips and immunofluorescence was performed to detect the levels of E-cadherin (red) in DMSO (D) and TRO (E) treated cells with DAPI (blue) stained nuclei. Values represent mean ± S.E.M. p value of ≤ 0.05 (*), n = 3 - 5.

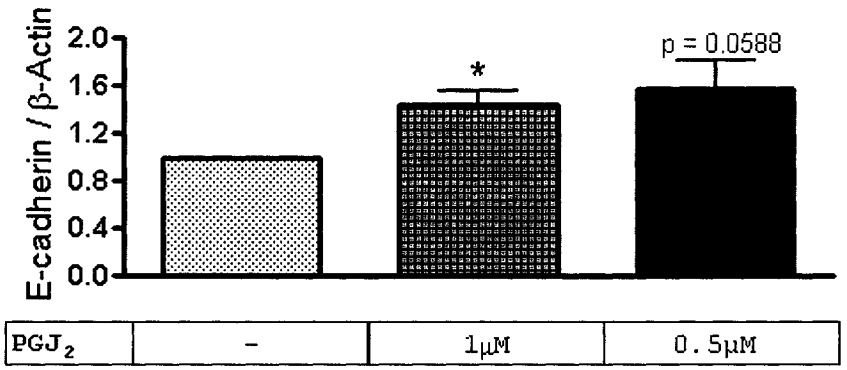

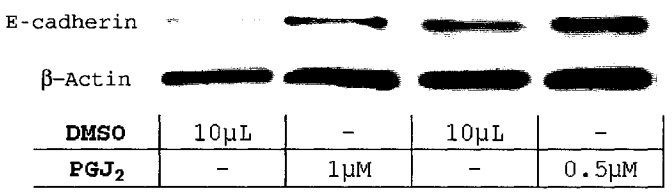

Fig. 10 - PGJ_2 increases E-cadherin expression in M1 cells

M1 cells were treated with PGJ_2 at concentrations of 0.5 & 1μM for 24 hours. E-cadherin protein levels were examined by Western Blot and normalized to β-actin. Values represent mean ± S.E.M. p value of ≤ 0.05 (*), n = 4 - 6.

A)

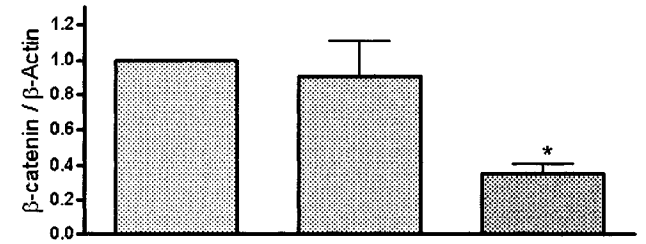

DMSO	10μL	-	-
TRO	-	5μM	10μM

DMSO	10μL	-	-
TRO	-	5μM	10μM

B)

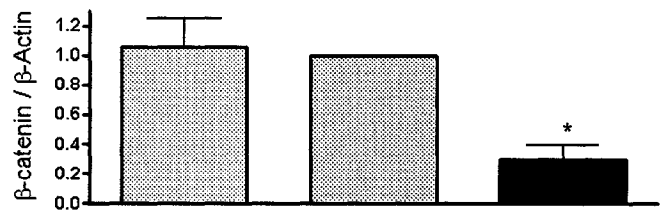

DMSO	-	10μL	-
TRO	-	-	5μM

DMSO	10μL	-	10μL	-
TRO	-	5μM	-	5μM

C)

D)

Fig. 11 - TRO attenuates β-catenin protein in IMCD-K2 & M1 cells
IMCD-K2 cells were treated with 5μM and 10μM of TRO & M1 cells were treated with 5μM of TRO, after 24 hour serum starvation. Western blot was performed for β-catenin and the results were normalized to β-actin (A & B). A band size of 94kDa was observed for β-catenin. Values represent mean ± S.E.M. p value of ≤ 0.05 (*), n = 3. M1 cells were also grown on cover-slips and immunofluorescence was performed to detect the levels of β-catenin (cyan) in DMSO (C) and TRO (D) treated cells at a magnification of 200X.

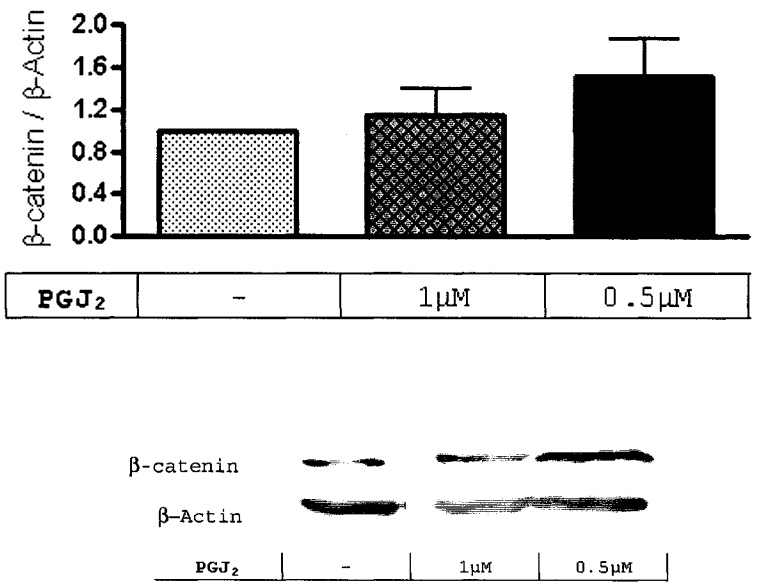

Fig. 12 - PGJ_2 increases β-catenin protein in M1 cells

M1 cells were treated with 0.5μM and 1μM PGJ_2, after 24 hour serum starvation. Western blot was performed for β-catenin and the results were normalized to β-actin. Values represent mean ± S.E.M.

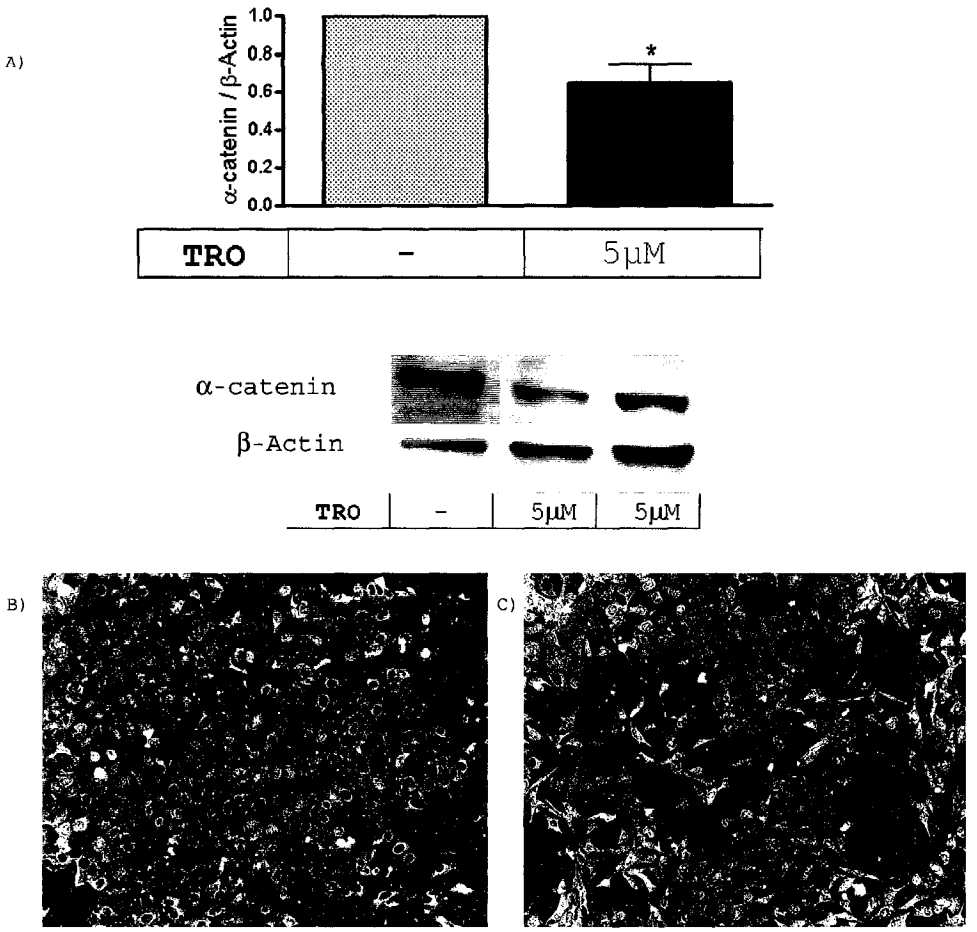

Fig. 13 - TRO attenuates α-catenin protein in M1 cells

M1 cells were treated with 5μM of TRO, after 24 hour serum starvation. Western blot was performed for α-catenin and the results were normalized to β-actin (A). A band size of 102kDa was observed for α-catenin. Values represent mean ± S.E.M. p value of ≤ 0.05 (*), n = 4. M1 cells were also grown on cover-slips and immunofluorescence was performed to detect the levels of α-catenin (yellow) in DMSO (B) and TRO (C) treated cells at a magnification of 200X.

A)

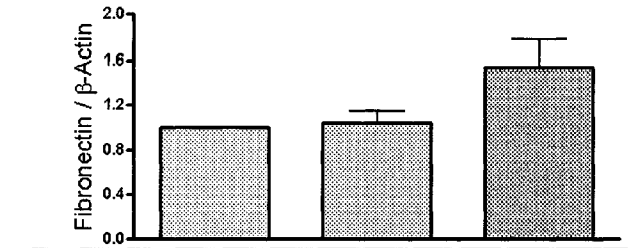

DMSO	10μL	-	-
TRO	-	5μM	10μM

DMSO	10μL	-	-
TRO	-	5μM	10μM

B)

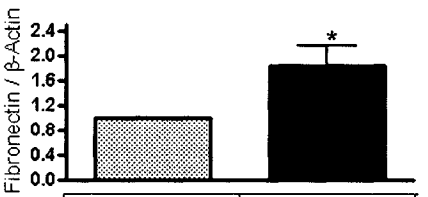

DMSO	TRO
10μL	5μM

DMSO	10μL	10μL	-	-
TRO	-	-	5μM	5μM

C)

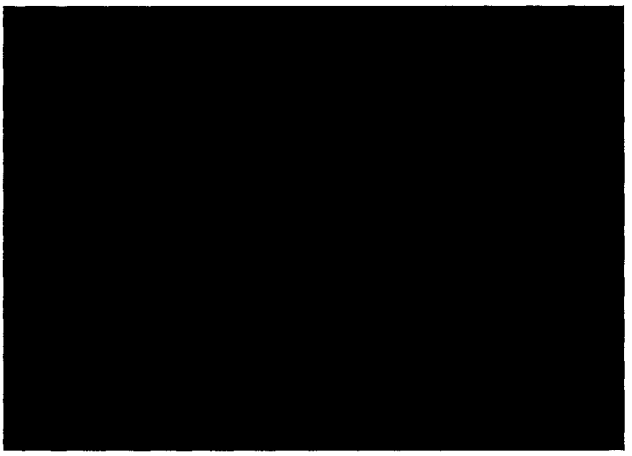

D)

Fig. 14 - TRO increases Fibronectin protein in IMCD-K2 & M1 cells
IMCD-K2 cells were treated with 5μM and 10μM of TRO (A) & M1 cells were treated with 5μM of TRO (B), after 24 hour serum starvation. Western blot was performed for Fibronectin and the results were normalized to β-actin (A & B). A band size of 220kDa was observed for Fibronectin. Values represent mean ± S.E.M. p value of ≤ 0.05 (*), n = 3 - 9. M1 cells were also grown on cover-slips and immunofluorescence was performed to detect the levels of Fibronectin (red) in DMSO (C) and TRO (D) treated cells at 200X magnification.

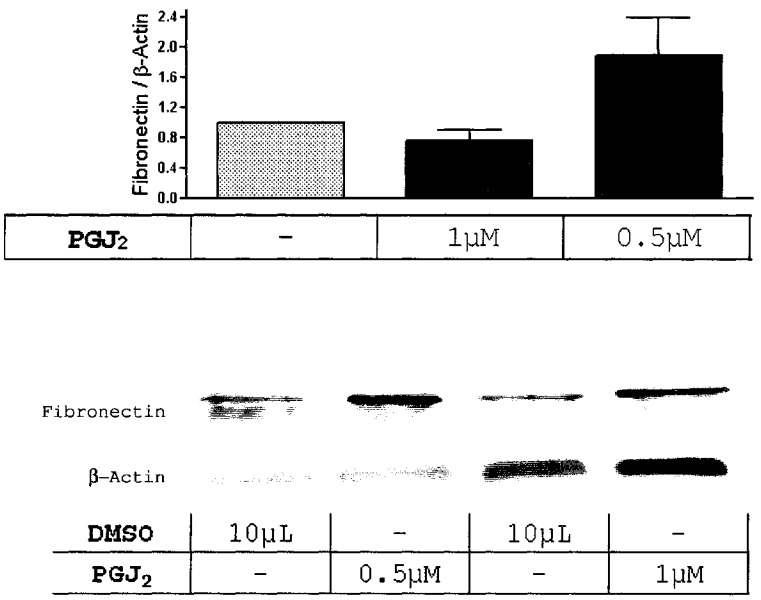

Fig. 15 - PGJ_2 increases Fibronectin in M1 cells

M1 cells were treated with 0.5μM, and 1μM PGJ_2, after 24 hour serum starvation. Western blot was performed for Fibronectin and the results were normalized to β-actin. Values represent mean ± S.E.M.

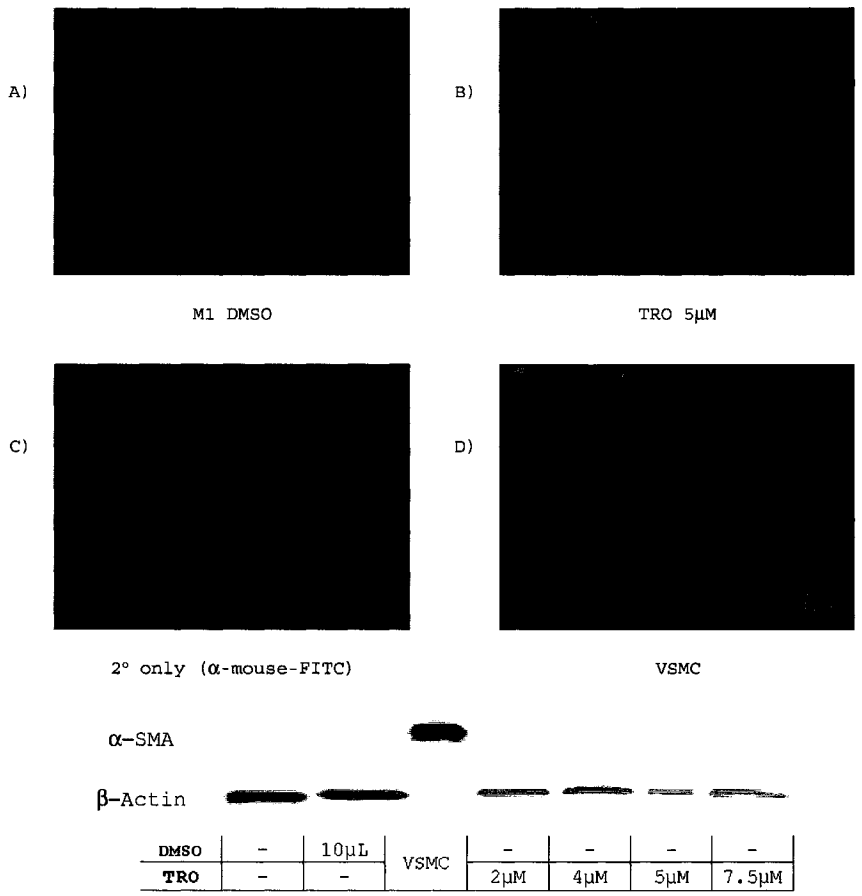

Fig. 16 - TRO does not increase α-SMA expression in M1 cells

M1 cells were treated with varying concentrations of TRO and Western blotting was performed for α-SMA (E), normalized with β-actin. M1 cells were also grown on cover-slips and stimulated with 5μM TRO for 24 hours. Immunofluorescence was used to observe α-SMA expression, visualized by the green FITC signal, in response to treatment (A & B). Vascular smooth muscle cells (VSMC) were also plated and probed with α-SMA as an experimental control (D) and the anti-mouse FITC-conjugated secondary treated cover-slip was used as a control for background (C) at 100X magnification.

3.4 TRO mediated effects in the M1 collecting duct cell line are primarily PPARγ independent

TZDs are known to induce several PPARγ-independent effects. The ~50% decreases in E-cadherin were not significantly attenuated with the PPARγ antagonist GW9662 or T0070907 (Fig. 17). In contrast, GW9662 showed a trend of attenuating the increase in E-cadherin with PGJ_2 stimulation however the differences were not statistically significant as the PGJ_2 experiments were variable (Fig. 18). The decreases in β-catenin were not reversed with GW9662 or T0070907 (Fig. 19), neither were the increasing trend in response to PGJ_2 (Fig. 20). The levels of α-catenin were further decreased, however not significantly, with T0070907 (Fig. 21). The increase in fibronectin was not significantly attenuated with the PPARγ antagonist GW9662 (Fig. 22a). Interestingly, there was a reversal in the 1.5-fold increase in fibronectin with T0070907 (Fig. 22b). GW9662 did not significantly attenuate the incrasing trend in fibronectin by PGJ_2 (Fig. 23).

The over-expression of PPARγ in M1 cells was performed to see whether an enhancement of the abovementioned effects could be observed. However, PPARγ over-expression did not significantly change the decrease in E-cadherin (Fig. 24) and increase in fibronectin (Fig. 25) compared to non-transfected cells and cells transfected with the plasmid control, not containing the PPARγ insert. Taken together these results portray a system in which PPARγ does not mediate the responses obtained from treatment with the synthetic ligand, TRO. The role of PPARγ in terms of fibronectin remains unclear however, due to the contradicting effects of the two antagonists GW9662 & T0070907.

A)

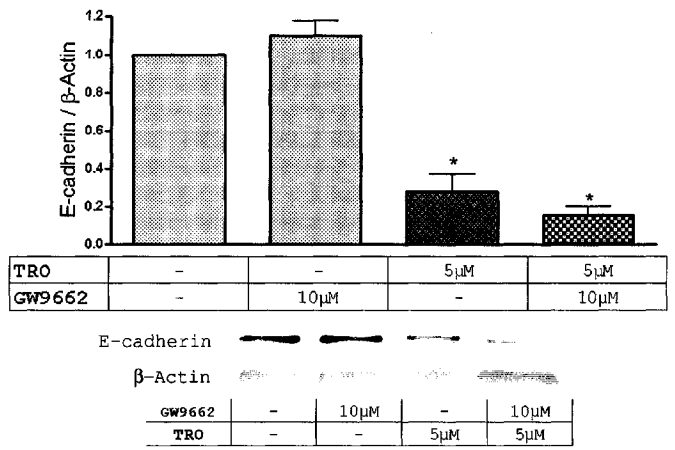

B)

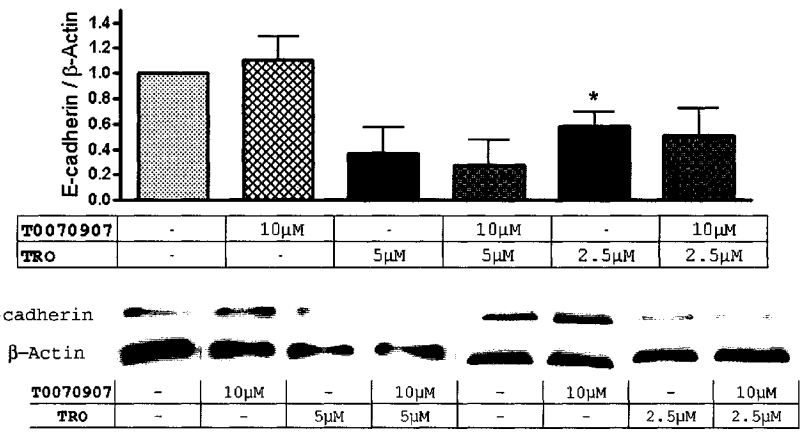

Fig. 17 - The decrease in E-cadherin by TRO is not reversed by the PPARγ antagonists GW9662 & T0070907

M1 cells were co-treated with 5μM TRO and either B)10μM T0070907 or A)10μM GW9662 for 24 hours. E-cadherin protein levels were examined by Western blot and normalized to β-actin. Values represent mean ± S.E.M. p value of ≤ 0.05 (*), n = 4.

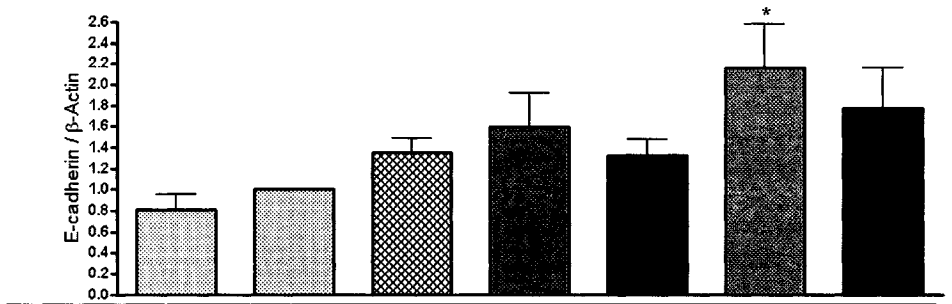

DMSO	-	10µL	-	-	-	-	-
PGJ_2	-	-	-	1µM	1µM	0.5µM	0.5µM
GW9662	-	-	10µM	-	10µM	-	10µM

PGJ_2	-	-	0.5µM	0.5µM	1µM	1µM
GW9662	-	10µM	-	10µM	-	10µM

Fig. 18 - GW9662 does not alter E-cadherin expression in response to PGJ_2

M1 cells were co-treated with 1µM or 0.5µM PGJ_2 and 10µM GW9662 for 24 hours. E-cadherin protein levels were examined by Western blot and normalized to β-actin. Values represent mean ± S.E.M. p value of ≤ 0.05 (*), n = 4 - 7.

A)

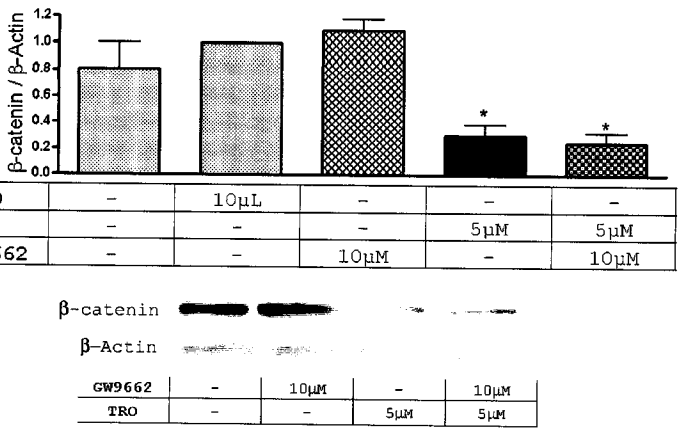

B)

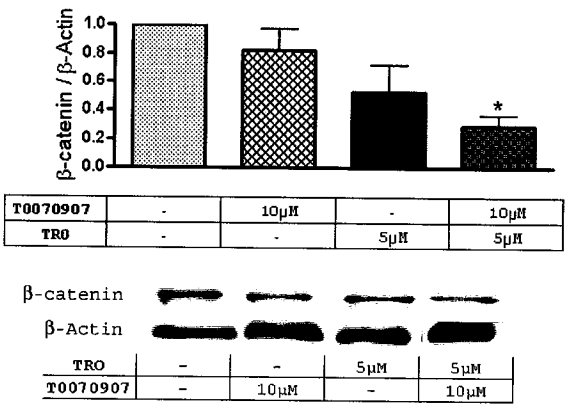

Fig. 19 - GW9662 & T0070907 do not reverse TRO decrease in β-catenin

M1 cells were co-treated with 5µM TRO and either 10µM T0070907 (B) or 10µM GW9662 (A) for 24 hours. β-catenin protein levels were examined by Western blot and normalized to β-actin. Values represent mean ± S.E.M. p value of ≤ 0.05 (*), n = 4.

C

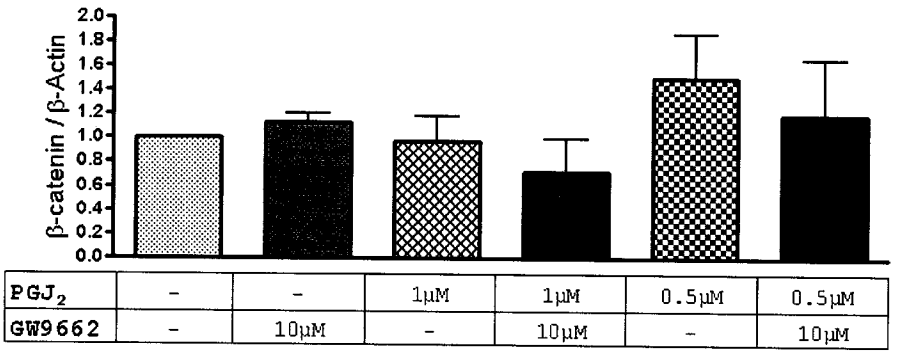

PGJ_2	-	-	1μM	1μM	0.5μM	0.5μM
GW9662	-	10μM	-	10μM	-	10μM

PGJ_2	-	-	1μM	1μM	0.5μM	0.5μM
GW9662	-	10μM	-	10μM	-	10μM

Fig. 20 - GW9662 does not alter PGJ2 effect on β-catenin

M1 cells were co-treated with 0.5μM or 1μM PGJ_2 and 10μM GW9662 for 24 hours. β-catenin protein levels were examined by Western blot and normalized to β-actin. Values represent mean ± S.E.M. p value of ≤ 0.05 (*), n = 4.

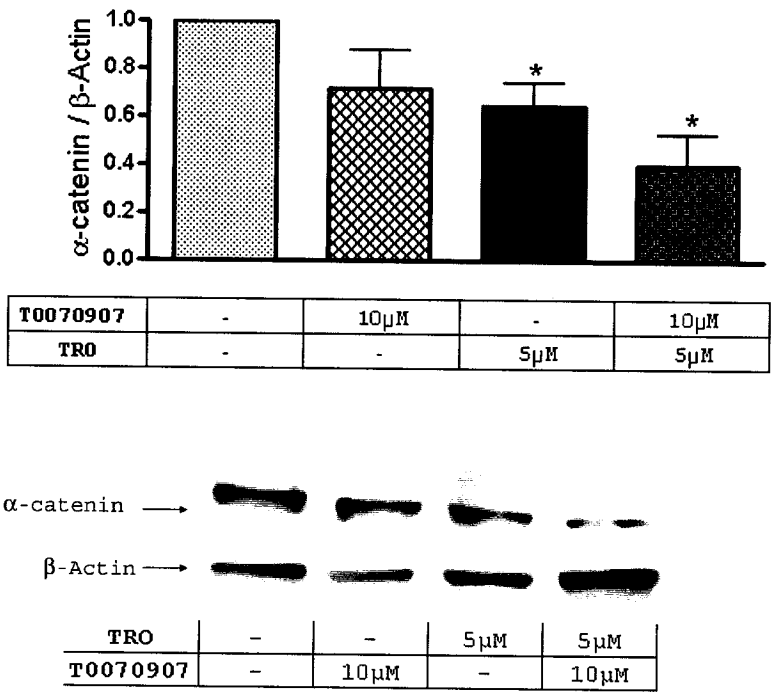

Fig. 21 - T0070907 does not reverse TRO-induced decreases in α-catenin

M1 cells were co-treated with 5μM TRO and 10μM T0070907 for 24 hours. α-catenin protein levels were examined by Western blot and normalized to β-actin. Values represent mean ± S.E.M. p value of ≤ 0.05 (*), n = 4.

A)

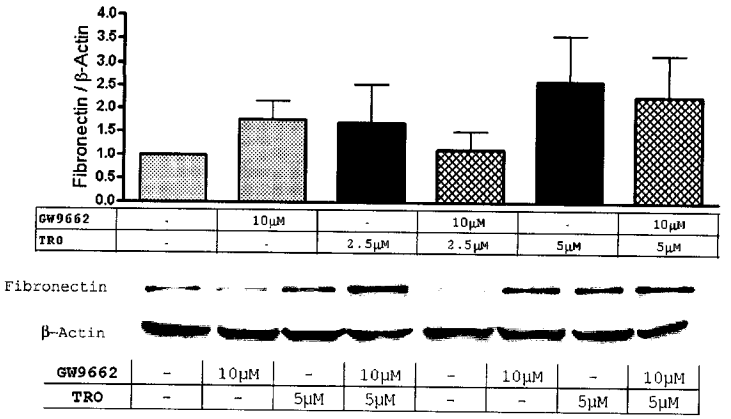

B)

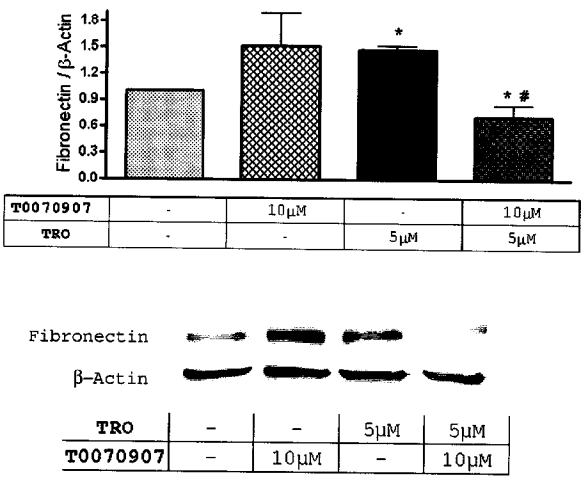

Fig. 22 - T0070907 abolishes TRO-mediated Fibronectin increase whereas GW9662 does not cause reversal

M1 cells were co-treated with 5μM TRO and either (A) 10μM T0070907 or (B) 10μM GW9662 for 24 hours. Fibronectin protein levels were examined by Western blot and normalized to β-actin. Values represent mean ± S.E.M. p value of ≤ 0.05 (*), n = 3 - 5. A two-tailed unpaired t test was also performed between [TRO] and [TRO + GW9662], or [TRO + T0070907] groups p value of ≤ 0.05 (#), n = 3 - 5.

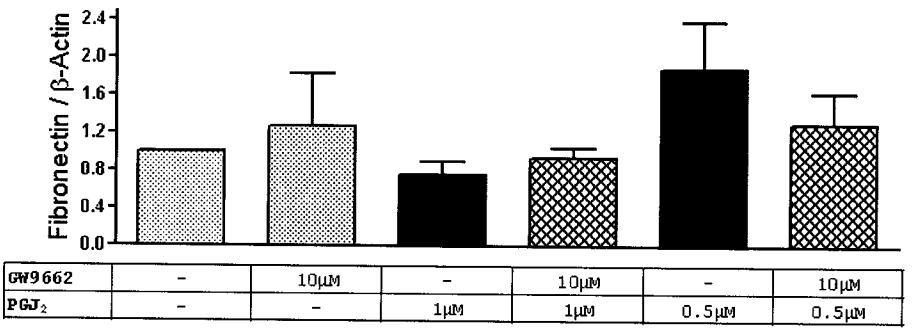

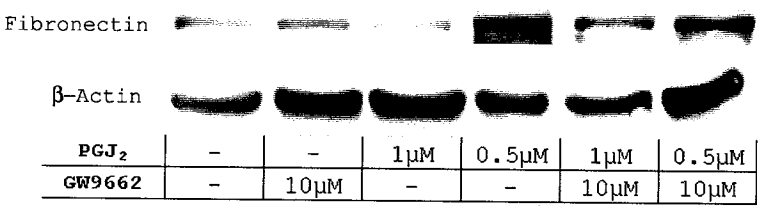

Fig. 23 - GW9662 does not alter the PGJ_2 effect on Fibronectin

M1 cells were co-treated with 1uM or 0.5uM PGJ_2 and 10μM GW9662 for 24 hours. Fibronectin protein levels were examined by Western blot and normalized to β-actin. Values represent mean ± S.E.M.

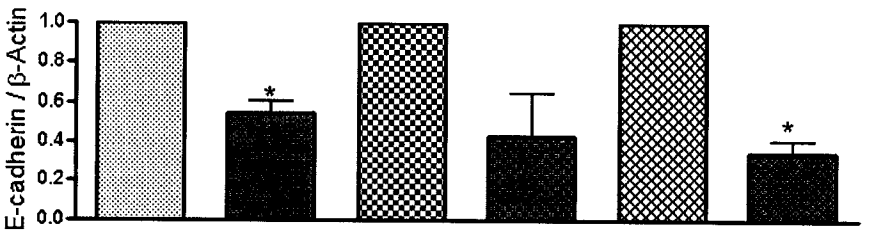

M1		pcDNA		pcDNA-PPARγ	
DMSO	TRO	DMSO	TRO	DMSO	TRO
10µL	5µM	10µL	5µM	10µL	5µM

M1		pcDNA		pcDNA-PPARγ	
DMSO	TRO	DMSO	TRO	DMSO	TRO
10µL	5µM	10µL	5µM	10µL	5µM

Fig. 24 - PPARγ overexpression does not alter TRO-induced reductions in E-cadherin

M1 cells were transfected with a pcDNA-PPARγ over-expression vector for 72 hours. The cells were stimulated with 5µM TRO for the last 24 hours of transfection. The levels of E-cadherin were compared in TRO treated cells to those of their respective controls. All values were normalized to β-actin and are presented as a fold control. Values represent mean ± S.E.M. p value of ≤ 0.05 (*), n = 3.

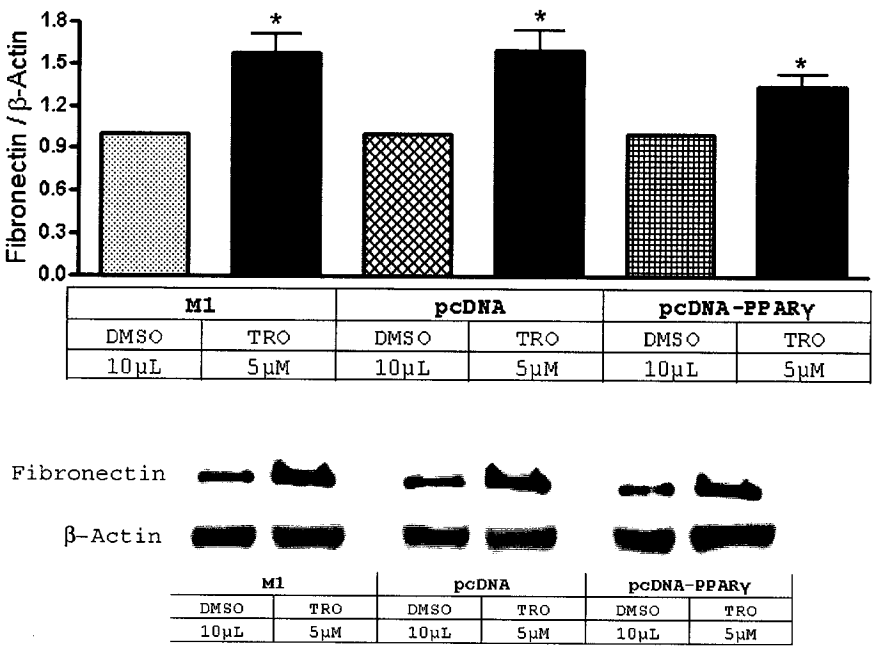

Fig. 25 - TRO increases Fibronectin in PPARγ overexpressing M1 cells
M1 cells were transfected with a pcDNA-PPARγ over-expression vector for 72 hours. The cells were stimulated with 5µM TRO for the last 24 hours of transfection. The levels of Fibronectin were compared in TRO treated cells to those of their respective controls. All values were normalized to β-actin and are presented as a fold control. Values represent mean ± S.E.M. p value of ≤ 0.05 (*), n = 3.

3.5 ECM / Cytoskeleton reorganization in the M1 collecting duct cell line by TRO is independent of the GSK-3β-APC-catenin degradation complex

We wanted to examine whether inhibiting the GSK-3β-APC-Catenin degradation complex could alter the increases in Fibronectin or degradation of the catenin-cadherin protein complex. GSK-3β phosphorylation is the crucial stage of one of the two APC dependent catenin degradation pathways. The GSK-3B inhibitor SB216763 did not reverse the decreases in E-cadherin (Fig. 26) and β-catenin, nor did it cause an increase in endogenous β-catenin levels (Fig. 27). The increase in Fibronectin was attenuated with SB216763 as the difference between the means was near significance at a p value of 0.0758 (Fig. 28). The decrease in α-catenin followed the same trend as the other epithelial markers with a further decrease with SB216763 & TRO (Fig. 29). LiCl, a second potential GSK-3β inhibitor, was able to increase total β-catenin levels at concentrations of 25mM & 50mM, unlike the synthetic GSK-3β inhibitor SB216763 (Fig. 34).

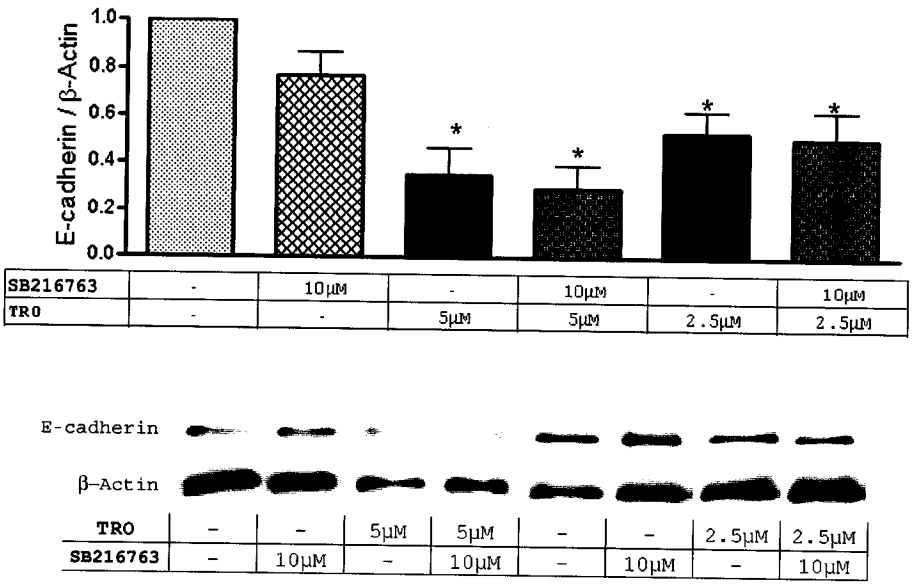

Fig. 26 - The GSK-3β inhibitor SB216763 does not reverse the TRO-induced decrease in E-cadherin

M1 cells were co-treated with 2.5μM or 5μM TRO and 10μM SB216763 for 24 hours. E-cadherin protein levels were examined by Western blot and normalized to β-actin. Values represent mean ± S.E.M. p value of ≤ 0.05 (*), n = 4.

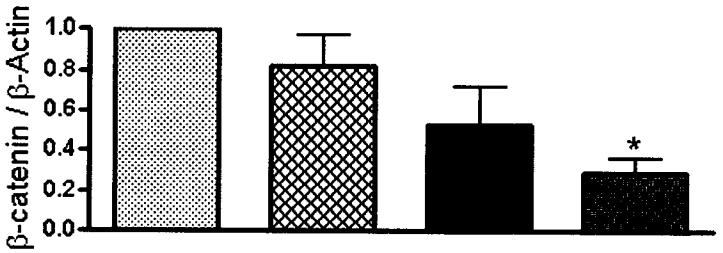

SB216763	-	10μM	-	10μM
TRO	-	-	5μM	5μM

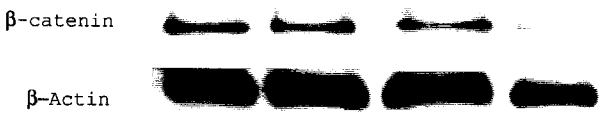

TRO	-	-	5μM	5μM
SB216763	-	10μM	-	10μM

Fig. 27 - The GSK-3β inhibitor SB216763 does not reverse the TRO-mediated decrease in β-catenin

M1 cells were co-treated with 5μM TRO and 10μM SB216763 for 24 hours. β-catenin protein levels were examined by Western blot and normalized to β-actin. Values represent mean ± S.E.M. p value of ≤ 0.05 (*), n = 4.

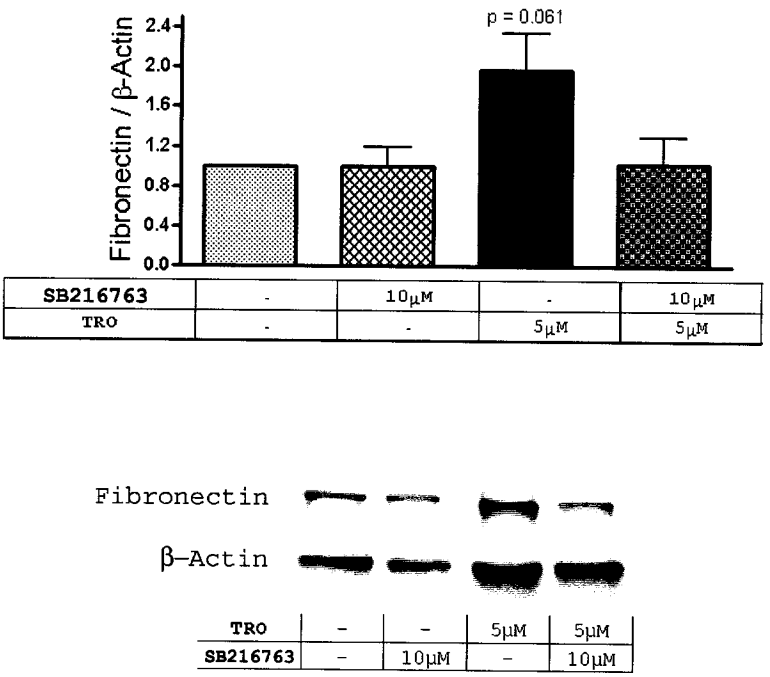

Fig. 28 - The GSK-3β inhibitor, SB216763, reverses the TRO-induced increase in Fibronectin

M1 cells were co-treated with 5μM TRO and 10μM SB216763 for 24 hours. Fibronectin protein levels were examined by Western blot and normalized to β-actin, observed at 220 KDa. Values represent mean ± S.E.M. p value of ≤ 0.05 (*), n = 4.

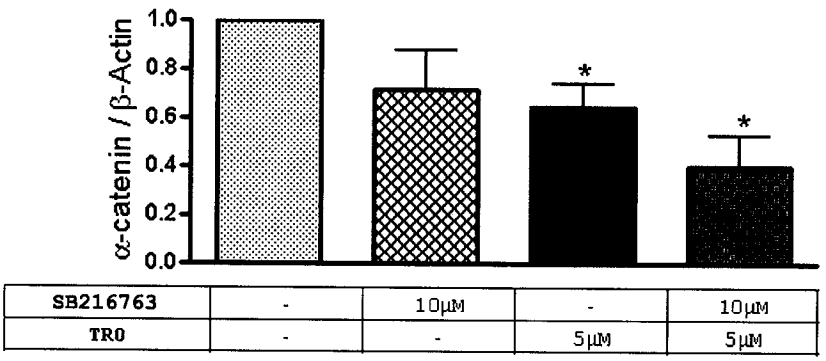

SB216763	-	10μM	-	10μM
TRO	-	-	5μM	5μM

TRO	-	-	5μM	5μM	5μM
SB216763	-	10μM	-	-	10μM

Fig. 29 - The GSK-3B inhibitor SB216763 does not reverse the TRO-mediated decrease in α-catenin

M1 cells were co-treated with 5μM TRO and 10μM SB216763 for 24 hours. α-catenin protein levels were examined by Western blot and normalized to β-actin, observed at 102 kDa. Values represent mean ± S.E.M. p value of ≤ 0.05 (*), n = 4.

3.6 Additional putative effects of TRO

ROS Assays were performed to verify whether the concentration of TRO caused an increase in H_2O_2 production, resulting in toxicity and possibly accounting for the effects observed. It was found that there was no increase in H_2O_2 between DMSO and TRO treated cells at any of the time points examined (Fig. 30). PGJ_2 had a tendency to cause a 40% reduction in endogenous H_2O_2 production. GW9662 had no effect on either PGJ_2 or TRO treated cells in terms of ROS generation.

The MAP kinases p38 and ERK were examined to test for PPARγ independent activation by TRO as their activation by TZDs has been published. Also MAP kinase activation has been shown to be capable of initiating the early stages of EMT. A 2-fold increase in phosphorylated p38 (Fig. 31) was observed however ERK1/2 was not activated (Fig. 32) with 5μM TRO stimulation. SMAD 2/3 protein was detected in the M1 cells. TRO did not significantly alter the total SMAD 2/3 protein levels when normalized to β-actin (Fig. 33) however this is not an appropriate measure of SMAD activity. SMADs are activated by phosphorylation, therefore the ratio of phosphorylated over total SMAD is required nonetheless this experiment was not performed for this study.

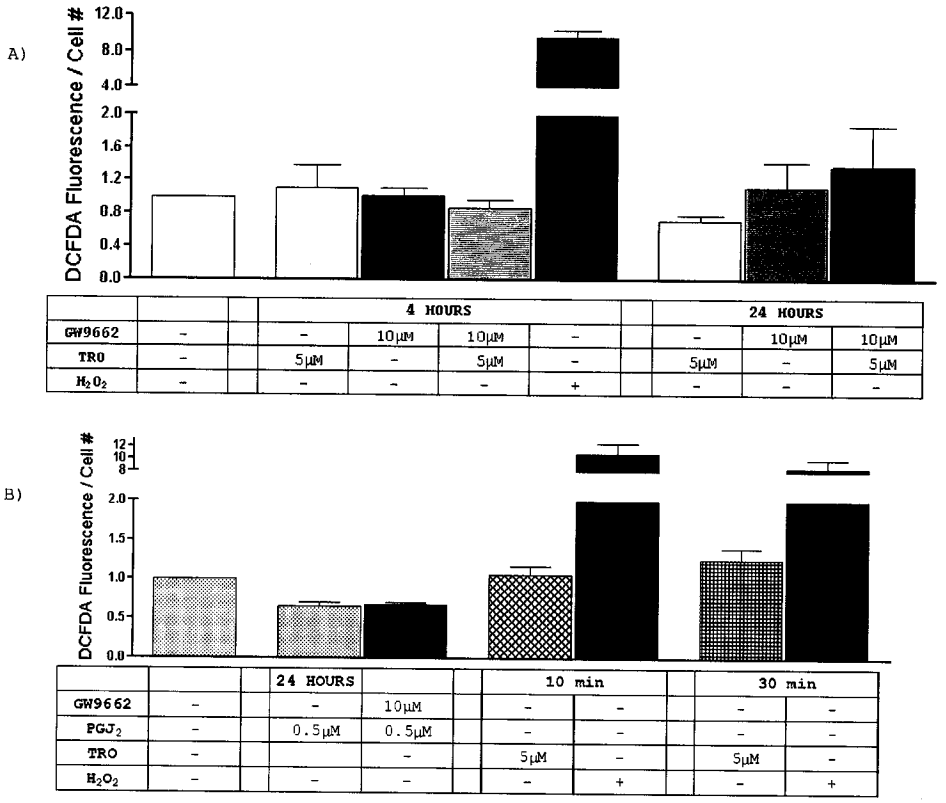

Fig. 30 - TRO does not increase H_2O_2 production in M1 cells

M1 cells were treated with DMSO, TRO, GW9662, 0.5μM PGJ_2, and H_2O_2 for 10 minutes, 30 minutes, 4 hours, and 24 hours. Cells were treated with 2μM DCFDA and the fluorescence was read with a fluorescence spectrophotometer with excitation and emission wavelengths of 485nm and 535nm. Fluorescence was normalized to the cell number and presented as a fold of DMSO treated cells. Values represent mean ± S.E.M. p value of ≤ 0.05 (*), n = 3 - 6.

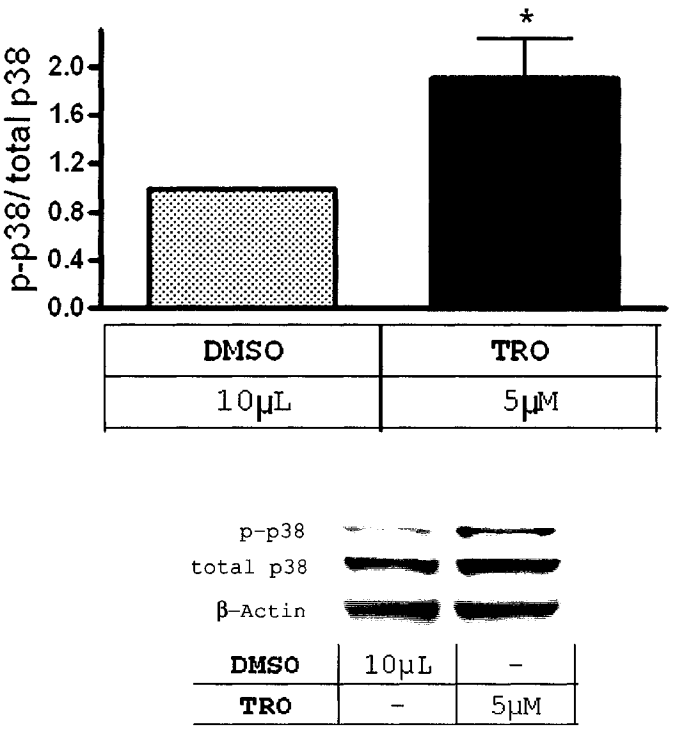

Fig. 31 - TRO increases p38 levels in M1 cells

M1 cells were grown to 65% confluence and treated with 5μM TRO for 24 hours, post 24 hour serum starvation. Protein was isolated, separated by SDS-PAGE and transferred to a nitrocellulose membrane where Western blotting was performed for phosphorylated p38, observed at 43kDa. Total p38 levels were used to normalize the results, presented as mean ± SEM. p value of ≤ 0.05, n = 6.

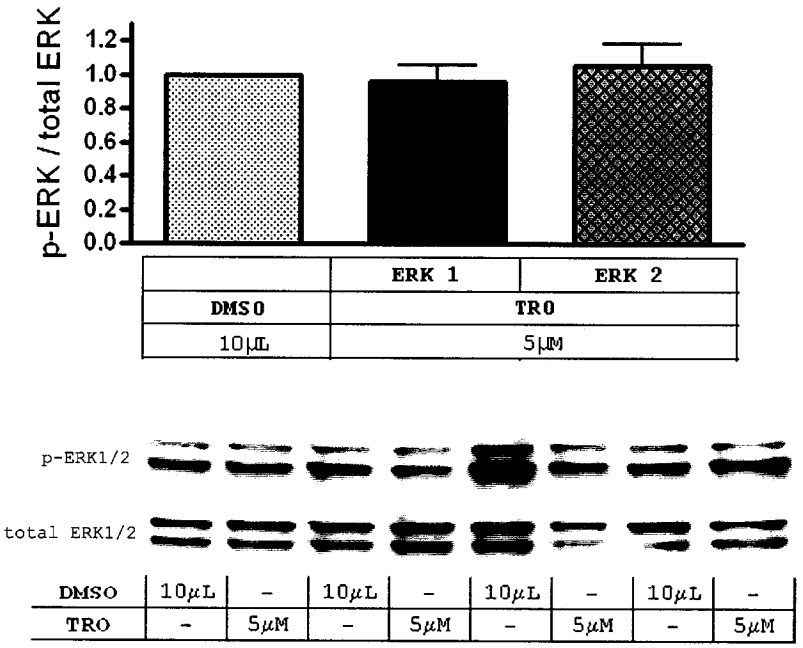

Fig. 32 - ERK is not activated by TRO in M1 cells

M1 cells were grown to 65% confluence and treated with 5µM TRO for 24 hours, post 24 hour serum starvation. Protein was isolated, separated by SDS-PAGE and transferred to a nitrocellulose membrane where Western blotting was performed for phosphorylated ERK 1/2, observed at 44kDa and ERK-2 at 42kDa. Total ERK 1/2 levels were used to normalize the results, presented as mean ± SEM. p value of ≤ 0.05, n = 6.

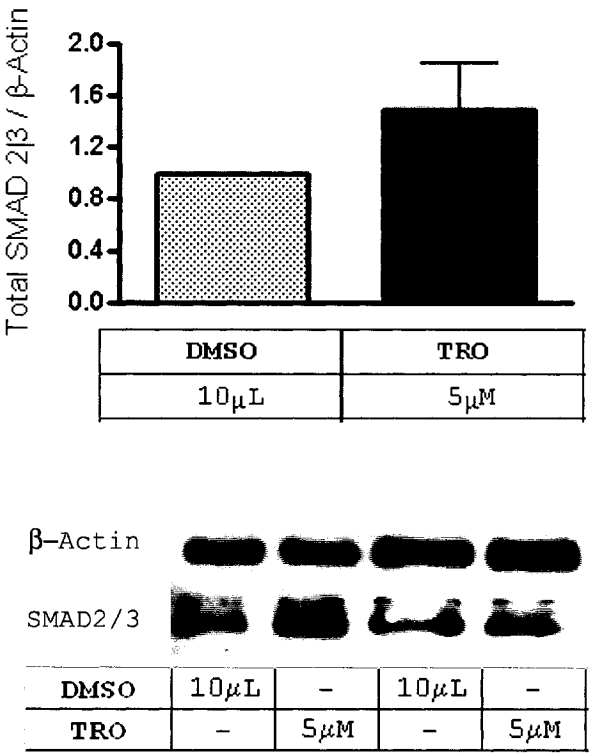

Fig. 33 - SMAD 2/3 are present in M1 cells and unchanged by TRO

M1 cells were grown to 65% confluence and treated with 5μM TRO for 24 hours, post 24 hour serum starvation. Protein was isolated, separated by SDS-PAGE and transferred to a nitrocellulose membrane and total SMAD 2/3 protein was analyzed by Western blotting. SMAD3 was observed at 52 kDa and SMAD2 at 60kDa. β-actin was used to normalize the results. Data presented as mean ± SEM, p value of ≤ 0.05, n = 6.

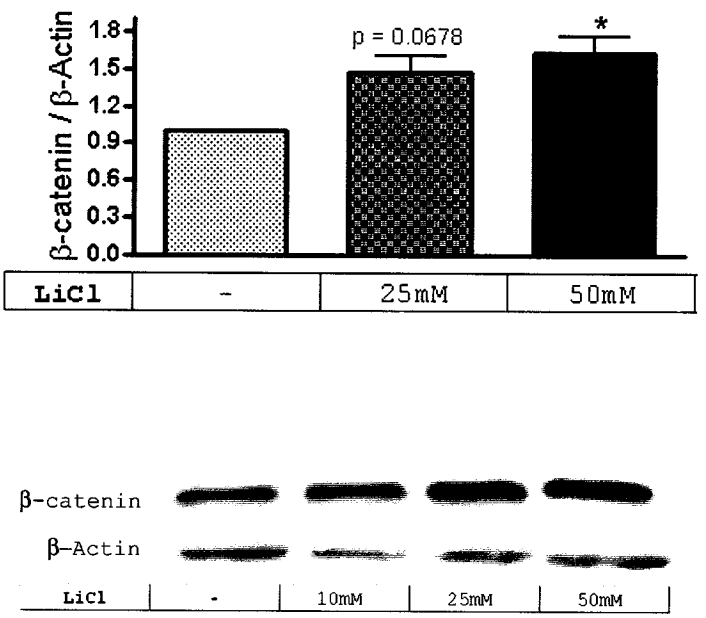

Fig. 34 - LiCl increases β-catenin protein in M1 cells

M1 cells were treated with 10mM, 25mM, and 50mM LiCl. Western blot was performed for β-catenin and the results were normalized to β-actin: p value of ≤ 0.05, n = 3.

4.0 Discussion

4.1 The TGF-β response in IMCD-K2 and M1 cells

An original goal of this study was to describe a fibrotic response in the collecting duct in terms of EMT and myofibroblast formation. TGF-β stimulation did not result in an epithelial to mesenchymal transition in either the cortical collecting duct M1 or IMCD-K2 cell lines as evidenced by the lack of morphological changes, the intact cell-cell adherens junctions, the maintenance of elevated E-cadherin levels and the lack of de novo α-SMA expression. Co-treatment with EGF, which has been shown to trigger a more pronounced epithelial transformation (Uttamsingh, Bao et al. 2008), (Wilkins-Port and Higgins 2007), did not initiate a fibrotic response either. Multiple time points were used in this study and prolonged exposure to both growth factors at high concentrations showed no signs of any initiation of a fibrotic response. In contrast, a mesenchymal transformation was induced in MCT proximal tubule cells as an increase in α-SMA and a spindle-like phenotype was observed.

The transformation of the MCT cells validates the activity of the TGF-β system used in these experiments. Endogenous TGF-β and receptor were previously characterized in both the IMCD-K2 and M1 cell lines as well (Husted and Stokes 1996), (Husted, Sigmund et al. 2000). SMAD2 and 3, the downstream effector molecules of TGF-β, were found in M1 cells and have been described in the IMCD (Uawithya, Pisitkun et al. 2008). The EGF receptor has also been characterized in the collecting duct (Falin, Veizis et al. 2005), (McEneaney, Harvey et al. 2007). It is possible that a longer time point may have resulted in a different outcome however the majority of experiments where EMT has been induced

used as little as 1ng/mL to 10ng/mL TGF-β for periods of 24 hours to 96 hours. Comparing this to our conditions and our treatment may appear excessive.

To my knowledge, the work presented in this thesis is the first attempt to characterize this phenomenon in these cell lines. Previous studies with TGF-β in IMCD-K2 and M1 cells have been published on the subject of electrochemical potential, electrolyte-ion exchange, and the renal ischemia / reperfusion injury model, but did not verify whether a fibrotic response was initiated in the cell lines upon cytokine stimulation (Husted and Stokes 1996), (Stokes 2000), (Han, Kim et al. 2007).

The necessary elements for a TGF-β response are present in both cell lines. Our data therefore suggests the regions representing the cell lines, namely the cortical and inner medullary collecting duct, do not contribute to myofibroblast formation in interstitial fibrosis as it is triggered by tubular EMT through cytokine stimulation (Radisky, Kenny et al. 2007). A migration pattern of damaged renal tubular epithelial cells, transformed into the more invasive mesenchymal phenotype, has been established in the proximal tubule (Saad, Gottlieb et al. 2002) and recently in a study using unilateral ureteral obstruction (UUO), a well-established model of severe renal interstitial injury, where intercalated cells expressing smooth muscle actin, had migrated through the basement membrane, contributing to the interstitial changes associated with poor prognosis (Butt, Tarantal et al. 2007). More recently, TGF-β and insulin-like growth factor induced a phenotypic transformation of the IMCD3 cells to a mesenchymal morphology with associated increases in vimentin and α-SMA with a

decrease in E-cadherin expression as early as 24 hour after stimulation (Ivanova, Butt et al. 2008). Given that intercalated cells are more abundant in M1 cells vs. IMCD-K2 (Boese, Aziz et al. 2004) or IMCD3 cells (Clapp, Madsen et al. 1987), one would expect that the M1 cell line would more readily undergo EMT. Our study refutes a suggestion of an intercalated cell-specific transformation in the collecting duct however the means by which the M1 and IMCD-K2 cell line do not transform remains unclear.

The immortalized state of the IMCD-K2 and M1 cells must be taken into consideration as they represent a closed system, however with the *in vivo* evidence emerging of collecting duct myofibroblast transformation, it must be considered that the IMCD-K2 and M1 cell lines' response to pro-fibrotic cytokines do not represent what may occur in intact tissue. Primary culture of collecting duct cells would be the best approach to distinguishing which segments could undergo EMT versus which segments show greater resistance, and help clarify the inconsistencies reported on collecting duct EMT.

4.2 PPARγ in the collecting duct & cell culture

PPARγ has been detected in vivo in the medullary & cortical collecting duct (Guan, Zhang et al. 1997) and was present in both IMCD-K2 and M1 cells. To my knowledge the only studies on PPARγ and the collecting duct indicate that it may be involved in sodium and fluid balance, as seen with the PPARγ knockout model reversing the edemic effects resulting from TZD treatment (Zhang, Zhang et al. 2005), (Guan, Hao et al. 2005). In our studies, the levels of PPARγ in M1 cells fluctuated, therefore we repeatedly examined the expression at different passages to ensure its presence during the length of the

study period. We also noted certain discrepancies in the responses to Troglitazone and PGJ_2 treatment between the initial studies and later experiments which may be attributed to passage number, and thus a new batch of M1 cells was used when passage numbers reached the late 60s. In spite of the fact that aliquots originated from the same stock, these freeze thaw cycles can be argued to cause variations in cell behaviour and response. As such, the statistical significance for the increase in Fibronectin, and decreases in E-cadherin and β-catenin were lost in some Troglitazone and PGJ_2 treated samples in experiments with the antagonists, inhibitors, and in overexpression studies, however the overall tendencies remained the same.

4.3 Troglitazone and cell morphology

TRO and PGJ_2 both appeared to slow cell growth with PGJ_2 treatment sometimes resulting in considerable cell death at concentrations higher than 1μM. TRO caused a loss in cell-to-cell contact and an elongated spindle-like phenotype in nearly half of the population of cells. The changes in cell shape appear to be PPARγ-independent as GW9662 did not restore the morphology or any cell-to-cell contact and occasionally resulted in a further disruption of cell integrity with TRO co-treatment. Any change in morphology resulting from TRO may be both PPARγ-dependent and -independent with the PPARγ independent pathway being capable of fulfilling the necessary steps to obtain the elongated phenotype. A PPARγ dependent pathway may also oppose the independent pathway where its inhibition may lead to a further phenotypic change. This elongated phenotype was not as distinct in populations that were able to reach confluence. This generally occurred if cells were stimulated with TRO at a confluence greater than 75%. Even with the

arrest in growth, highly populated plates were able to proliferate in close proximity. Decreases in E-cadherin and β-catenin were still obtained for a few of these "over-confluent" plates. However the data was not included with the results from plates where cells had become elongated and phenotypically different to minimize variability. Nonetheless, this observation leads to the question of whether the morphological changes correlate directly with the ECM and cytoskeletal changes in response to TRO. The fact that a confluent dish of TRO treated M1 cells still undergoes the same catenin-cadherin degradation suggests morphology is independent of adheren junction integrity, but rather appears to be partially dependent on cell density and other cell contact factors.

Accordingly, TGF-ß1 was unable to induce EMT in intact confluent monolayers of tubular epithelial cells, however loss of epithelial integrity (sub-confluence, wounding, and contact disassembly by Ca^{2+}-removal) restored its EMT-inducing effect (Masszi, Fan et al. 2004). A cell contact-dependent regulation of epithelial-myofibroblast transition via the rho-rho kinase-phospho-myosin pathway has also recently been described (Fan, Sebe et al. 2007). TGF-β stimulation of firmly intact epithelial layers does not appear to be able to alter morphology and initiate cell-to-cell contact disruption similarly to TRO and the confluent layers of IMCD-K2 and M1 cells.

Despite the lack of response to TGF-β, we did detect a small trend for an increase in total SMAD2/3 protein in response to TRO. SMADs are crucial in TGF-β related morphological changes and the over-expression of SMAD3 resulted in a more pronounced change in morphology in adipocyte differentiation (Choy, Skillington et al. 2000).

Interactions between PPARγ and TGF-β/Smad2/3 signalling pathways have been published (Hao, Niu et al. 2008), although cross-communication of TGF-β/Smad signal to the Wnt/β-catenin/TCF4 pathway has been shown to lead to the down-regulation of PPARγ (Guo, Flanagan et al. 2008). Nonetheless, the morphological changes could have been mediated by SMAD2/3 downstream of TGF-β and an increase in total SMAD2/3 may have signified the initiation of a morphogenic response.

PI3 kinase-dependent Akt phosphorylation and intracellular calcium are two key signalling processes known to be involved in the regulation of cytoskeleton remodeling. Akt activation increased in response to PGJ_2 and TRO in vascular smooth muscle cells (Atkins, Northcott et al. 2005). Rosiglitazone was also shown to modulate actin remodeling in monocytes independently of PPARγ activation and influenced by Akt and intracellular calcium (Singh, Webb et al. 2005). It would be useful to verify whether Akt phosphorylation by PI3 kinase is increased in collecting duct cells upon stimulation with TRO and whether PI3 kinase's inhibition would attenuate any changes in cellular morphology or physiology.

4.4 Troglitazone and PPARγ independent MAPK activation

Nuclear receptors are not always dependent on ligand binding for gene activation, but can also be regulated by post-translational events, such as phosphorylation, that may be brought about by interactions with a diversity of signalling transduction pathways including MAPK, PI3K/Akt, and Wnt. Furthermore, several studies using TZDs have characterized PPARγ-independent effects, primarily through the activation of MAP kinases, namely, ERK1/2, p38, JNK/SAPk, PI3, and Akt (Berger, Leibowitz et al. 1999), (Xing, Xin et al. 2008), (Rosa,

Egea et al. 2008), (Schiefelbein, Seitz et al. 2008). PGJ_2 has also been shown to act independently of PPARγ through the activation of tyrosine and MAP kinases in the kidney (Kimura, Li et al. 2008). MAPK activation has been shown to be necessary and sufficient to induce the primary stages of partial EMT (Hellman, Spector et al. 2008). Although ERK1/2 was not activated, p38 phosphorylation was increased by TRO. This MAPK activation may have been sufficient to induce the changes in morphology and possibly the ECM / cytoskeleton observed in our studies as it has been suggested that the p38 MAPK pathway contributes to EMT and cell migration (Bakin, Rinehart et al. 2002). Other MAP kinases may also be activated by Troglitazone in the IMCD-K2 and M1 cell lines, as has been shown in other studies (Kim, Yoo et al. 2006), (Gardner, Dewar et al. 2003), (Goetze, Kintscher et al. 2001)).

Although ERK was not activated in our studies, a link between EMT and PPARγ has been established in intestinal epithelial cells, with PPARγ promoting epithelial to mesenchymal transformation *via* the activation of ERK1/2 (Chen, Necela et al. 2006). ERK has been shown to be able to induce the initial stages of EMT (Javle, Gibbs et al. 2007) however the intestinal transformation by PPARγ showed no formation of pronounced actin stress fibers, similarly to our study. We believe the observed transformation with no increased α-SMA expression should be referred to as "partial-EMT or truncated-EMT" as described in other studies (Feige, Gelman et al. 2006), (Chen, Halberg et al. 2008), (Hellman, Spector et al. 2008).

4.5 Troglitazone and Reactive Oxygen Species generation

There was no significant increase in ROS production by Troglitazone in M1 cells, indicating the effects described in this study are independent of increased ROS production and subsequent MAPK activation. This is not to say that Troglitazone could not activate the MAPK signalling pathway through other means. Nonetheless, PPARγ agonists have been shown to have cytotoxic effects at high concentrations in renal proximal tubular cell lines (Giral, Villa-Bellosta et al. 2007). In rat glioma cells, mouse GL261 glioblastoma cells, and primary astrocytes it was found that Troglitazone resulted in increased apoptosis, decreased mitochondrial membrane potential, and increased radical oxygen species production (Feinstein, Spagnolo et al. 2005) whereas 15d-PGJ_2 induced cell death through the mitochondrial apoptotic pathway dependent on ROS and JNK activation in osteoblastic cells (Lee, Kim et al. 2008). ROS generation has been shown as a side effect of other TZDs, conversely PPARγ has also been shown to have a protective effect, promoting cell survival against ROS generation (Jo, Yang et al. 2006), (Yang, Jo et al. 2007).

E-cadherin, as well as other structural stabilizing proteins, have been shown to be reduced by ROS induction in tumour tissue (Thews, Lambert et al. 2007). The relation between ROS generation and tumour stability and metastasis suggested a possible role for TRO related ROS generation altering collecting duct cell morphology and E-cadherin levels. Although the evidence for this link is weak, we felt it was important to verify whether an increase in ROS production occurred with TRO treatment as reactive oxygen species are involved in TGF-β signalling, are upstream signalling molecules to several MAP kinases,

and H_2O_2 was able to reproduce some of the effects of TGF-β in proximal tubular epithelial cells (Rhyu, Yang et al. 2005).

4.6 Troglitazone and the ECM / cytoskeleton

Troglitazone induced decreases in several epithelial adhesion markers such as E-cadherin, α-catenin, and β-catenin, caused an upregulation of Fibronectin, but did not trigger *de novo* α-SMA expression. PGJ_2 on the other hand increased E-cadherin, β-catenin, and Fibronectin levels.

4.6.1 E-cadherin

The decrease in E-cadherin in response to Troglitazone was the major effect characterized in both IMCD-K2 and M1 cells. An increase in E-cadherin, as seen with PGJ_2 treatment, was expected due to E-cadherin's functional PPRE and several studies where PPARγ agonists increased E-cadherin expression (Annicotte, Iankova et al. 2006). The decrease resulting from TRO stimulation may still involve the PPAR response element, since a PPARγ co-repressor complex could have bound to E-cadherin's PPRE, preventing further transcription and thereby translation of the E-cadherin protein. A core function of p120-catenin is to regulate cadherin stability and turnover by controlling cadherin entry into the degradative endocytic pathways (Desclozeaux, Venturato et al. 2008), (Reynolds and Carnahan 2004). The decrease in protein levels could have been due to enhanced E-cadherin turnover and degradation. This theory would require a closer look at p120-catenin and would require inhibiting its ability to mediate the degradation of E-cadherin through the aforementioned pathway. If E-cadherin levels remained constant with p120-catenin inhibition and TRO treatment in the

IMCD-K2 & M1 cells, this would indicate the decreases observed in our study were a result of an internal cadherin degradation system where TRO prevented regeneration of E-cadherin protein.

Additional studies which show an increase in E-cadherin include MCF-7 breast cancer cells treated with conjugated linoleic acid, which acts as a PPARγ agonist, causing an up-regulation and redistribution of β-catenin and E-cadherin (Bocca, Bozzo et al. 2007). An up-regulation of E-cadherin by TRO in xenograft tumour tissues independently of PPARγ has also been published (Qiao, Dai et al. 2008). The decrease in E-cadherin in our study occurs independently of PPARγ as well. The PPARγ antagonists T0070907 and GW9662 did not reverse the decrease observed. Over-expression of PPARγ did not alter E-cadherin levels upon TRO stimulation either. Also the opposing effects of the two agonists, TRO and PGJ_2, create another argument that the effects of at least one of the ligands are PPARγ-independent. Another explanation is that one ligand activates PPARγ at a higher capacity than the other as PPARγ activation may induce opposing effects depending on the magnitude of PPARγ activation (Clay, Namen et al. 2001). The GSK-3β inhibitor SB216763 did not reverse E-cadherin levels either; however this was expected as GSK-3β specifically phosphorylates β-catenin for degradation and no direct relation between cadherins and the GSK-3β degradation complex has been published to date.

4.6.2 β-catenin

TRO caused a decrease in β-catenin in IMCD-K2 & M1 cells. This decrease was not reversed by the PPARγ antagonists GW9662 & T0070907 or the GSK-3β inhibitor SB216763. β-catenin degradation generally occurs through the adenomatous polyposis coli (APC) tumor-suppressor protein,

together with Axin and GSK-3β, forming a Wnt-regulated signalling complex that mediates phosphorylation-dependent degradation of β-catenin by the proteasome, as well as an APC/Siah-1 mediated degradation pathway linking p53 activation to cell cycle control (Liu, Stevens et al. 2001). The GSK-3β inhibitor SB216763 was therefore expected to increase endogenous β-catenin levels, however it did not, showing a trend for a slight decrease. Dose responses showed concentrations higher than the 10μM used were detrimental to cell growth and ranges higher than 30μM resulted in toxicity and cell death. LiCl has also been shown to increase β-catenin levels and interfere with GSK-3β phosphorylation of β-catenin (Li, Lee et al. 2006). The increase in β-catenin induced by 25mM and 50mM LiCl in M1 cells is noteworthy as future experiments may be performed to verify whether LiCl can attenuate Troglitazone's degradation of β-catenin (Fig. 34). Lithium is known to inhibit GSK-3β activity by acting as a competitive inhibitor of Mg^{2+} and by increasing inhibitory phosphorylation at Ser-9 through activation of the Akt/protein kinase B pathway (Ryves and Harwood 2001) whereas SB216763 inhibits GSK-3β in an ATP-competitive manner. The potency of Lithium inhibition is dependent on Mg^{2+} concentration as opposed to ATP, suggesting in M1 cells ATP levels exceed those allowable for its competitive inhibition.

PPARγ activation has been shown to induce the proteasomal degradation of β-catenin as well as a reduction in E-cadherin in hepatocytes (Sharma, Pradeep et al. 2004). PPARγ has been shown to target β-catenin to the proteasome through its catenin binding domain (CBD), by means of its phosphorylation at the N terminus by GSK3β (Liu and Farmer 2004), (Chou, Wang et al. 2007), as well as through a novel APC/GSK3β/p53-independent ubiquitination-mediated proteasomal

degradation pathway (Sharma, Pradeep et al. 2004). The novel APC-independent mechanism remains unclear but proteasomal inhibitors have been shown to reverse the effects of TZDs on β-catenin, indicating the involvement of the proteasome in the process. It would be interesting to see if the decreasing β-catenin and E-cadherin levels in our study could be restored with a protease inhibitor in collecting duct cells upon stimulation with Troglitazone.

A similar pathway, independent of APC has also been recently characterized in the degradation of β-catenin with RXRα agonist treatment (Dillard and Lane 2008), (Dillard and Lane 2007). RXRs being the heterodimer partner of PPARs suggest a similar APC-independent pathway could be described in the collecting duct with TZDs. An interaction between RXRα and β-catenin, in the absence of ligand, has been shown *in vivo* with RXR agonists enhancing this interaction (Xiao, Ghosn et al. 2003). It is possible that TRO may activate to a lesser extent some RXR-dependent pathways, or *vice versa* with RXR agonists activating PPAR activity as well. RXR agonists are capable of targeting specific heterodimer pairs while discriminating similar RXR/PPAR heterodimer partners in the same system (Leibowitz, Ardecky et al. 2006) therefore certain agonists specifically target the PPARγ/RXRα transcription complex. Further research into the precise nature of the PPARγ/RXRα heterodimer may advance the understanding of this cross-talk between respective agonists as is seen in cancer treatment where the synergistic effects of PPARγ ligands and retinoids have been characterized (Tsujie, Nakamori et al. 2003), (Shimizu and Moriwaki 2008).

Interestingly, the TZD NP00111 has been shown to inhibit GSK-3β activity in a non-competitive manner to ATP (Rosa, Egea et al. 2008). This presents another example of opposing effects within TZD use, as an inhibition of GSK-3β activity by Troglitazone in the M1 and IMCD-K2 cells would have resulted in a decrease in β-catenin phosphorylation and a subsequent increase in β-catenin levels. Theoretically, the inhibitor SB216763 and Troglitazone would have both increased β-catenin levels, yet when administered separately or together, no such increase was observed (Fig. 15). PGJ_2 was able to induce an increase in β-catenin levels, contradicting the abovementioned effects of PPARγ activation and β-catenin degradation. It should be noted however that many of the studies published on this topic assume that PPARγ agonist use is sufficient to activate the receptor. Additionally, the fact that SB216763 was not able to prevent endogenous catenin degradation is disappointing as the legitimacy of the drug as a GSK-3β blocker in M1 cells must be questioned. A GSK-3β activity assay would verify whether there was a change in GSK-3β activity and would validate the efficiency of the inhibitor as well.

4.6.3 α-catenin

TRO caused a decrease in α-catenin in M1 cells. This decrease was not reversed by T0070907 or SB216763. This suggests the degradation of α-catenin to be independent of PPARγ activation as well as independent of GSK-3β. The α-catenin protein has been shown to exist as a monomer or a dimer with monomeric α-catenin binding more strongly to E-cadherin-β-catenin and the dimer preferentially binding to actin filaments (Drees, Pokutta et al. 2005). The proportion of monomeric to dimerized α-catenin affected by TRO stimulation may shed light on the

local regulation of actin assembly and organization at sites of cadherin-mediated cell-cell adhesion.

4.6.4 Fibronectin

Fibronectin was upregulated in the presence of TRO and PGJ_2. GW9662 did not reverse the TRO-mediated increase in FN however T0070907 and SB216763 were able to attenuate the effect. Both PPARγ anatagonists produced contradictory effects; however the over-expression of PPARγ did not affect the increase in FN, suggesting an overall PPARγ-independent effect. Interestingly, GW9662 and T0070907 alone had a tendency to increase Fibronectin as well. Generally TZDs reverse fibronectin expression in diseased states, such as human lung carcinoma cells (Han, Ritzenthaler et al. 2005), in human cortical fibroblasts (Zafiriou, Stanners et al. 2005), in TGF-β treated glomerular mesangial cells (Guo, Koya et al. 2004), and in diabetic mice (Qin, Li et al. 2006).

An inhibition of PPARγ could in theory cause an increase in Fibronectin if the true role of PPARγ was a protective one, attenuating fibronectin levels even in a normal state. This would be reflected by the aforementioned increases in fibronectin upon GW9662 and T0070907 treatment. Troglitazone could therefore be causing an increase in FN independent of PPARγ as the data suggests. Even so, the fact that one of the PPARγ antagonists reversed the increase in FN is perplexing and contradicts our conclusion that these effects are mainly independent of PPARγ activation in these cell lines. Further studies are needed to clarify the underlying mechanisms however the fact that T0070907 mediates its effects through preventing PPARγ co-activator recruitment while GW9662 acts through its ability to prevent PPARγ ligand binding

suggests the increase in Fibronectin could be dependent on a PPARγ co-activator.

Interestingly, β-catenin has been shown to target a functional LEF/TCF binding element in Fibronectin's promoter region thereby increasing its expression in a WNT-dependent manner in fibroblasts (Zhai, Wu et al. 2002). An increase in Fibronectin was not expected with the GSK-3β inhibitor SB216367, due to the predicted increases in β-catenin levels, as the Fibronectin promoter was silent in the epithelial cells examined (Gradl, Kuhl et al. 1999). Nevertheless, if a functional FN promoter with an intact LEF/TCF binding site was present in IMCD-K2 & M1 cells, an increase in β-catenin could have correlated with an increase in Fibronectin. These trends were observed with PGJ_2 treatment, where increases in β-catenin correlated with those of Fibronectin. In spite of this, the opposite effect was observed in M1 cells as the increase in Fibronectin was essentially reversed by the GSK3 inhibitor. The mechanism by which SB216367 is acting may stem from its nature as an ATP competititor however further studies are required.

4.7 Summary

Modulations in the components of the ECM & cytoskeleton, specifically the cadherin-catenin complex, have not been well characterized in the kidney with the exception of a few studies examining the formation and maintenance of adheren junctions, as well as the ischemia-induced degradation of E-cadherin observed in renal epithelial cells (Bush, Tsukamoto et al. 2000). PPARγ's interaction with E-cadherin and β-catenin has not been described in the kidney, as the majority of the literature is in the field of cancer research. Furthermore no link between the other PPAR isoforms and cadherin-

catenin degradation has been established, suggesting only the PPARγ isoform is capable of producing the effects characterized in our study.

Twenty-four hour TRO stimulation of IMCD-K2 and M1 immortalized collecting duct cells caused morphological changes associated with decreases in E-cadherin, β-catenin, and α-catenin independently of PPARγ, as well as an increase in Fibronectin. The p38 MAP kinase was also activated and may have contributed to the matrix rearrangement observed. There was no increase in actin stress fiber formation and these effects were independent of TGF-β as the cytokine was unable to induce EMT in both cell lines.

The characterization of additional mesenchymal markers such as N-cadherin and vimentin may aid in distinguishing whether TRO is capable of causing EMT in collecting duct cells, as they are increased in response to TGF-β. Also, a comparison between nuclear and cytoplasmic β-catenin levels in response to TRO would elucidate whether a decrease in LEF/TCF gene activation through β-catenin transcriptional activity occurred. Focal adhesion proteins, including ZO-1, vinculin, integrin β1, and focal adhesion kinase could also play a factor.

The discovery of novel gene targets for PPARγ ligands could prove to be useful in identifying commonly agonist-induced PPARγ independent pathways as well and may elucidate whether specific downstream fibrotic or anti-fibrotic signalling factors are activated by any of the agonists, leading to an improved and more specific understanding of the beneficial effects as well as side-effects of these popular drugs.

4.8 Conclusion

The difficulty in trying to reverse the effects caused by TRO in these studies was to find a pathway consistent with the results obtained and to target it at the site where TRO would be initiating its progression. EMT was a likely candidate as the only studies where all three major effects were observed, namely the decreases in E-cadherin & β-catenin and increase in FN, involve EMT. Yet TGF-β was not able to induce a mesenchymal transformation in either cell line shedding some doubt on this theory. Proteasomal degradation appears to explain the decreases in E-cadherin and catenins. This study, along with others recently published, may be portraying the activation of a novel proteasomal pathway where PPARγ ligands are capable of triggering the degradation of proteins involved in regulating important cellular events such as growth and differentiation. The possibility that all the described effects are independent of one another and independent of PPARγ activation must be considered. There is some contradicting data with FN suggesting the increase in fibronectin may be PPARγ and GSK-3β dependent but it seems a PPARγ independent pathway is more likely.

TRO may be acting upon multiple pathways, triggering several cascades that contribute to the end effects. It would be difficult to prevent or inhibit the numerous targets along the chain. In terms of Occam's razor, a PPARγ dependent mechanism would have been the simplest and most probable explanation as the nuclear receptor has been shown to interact with members of the cadherin-catenin cytoskeleton complex through the functional PPRE described in E-cadherin, as well as its catenin binding domain (CDB) which interacts directly with the TEC/LCF domain in β-catenin. Antagonism of PPARγ activity would have thus

prevented the degradation of the cadherin-catenin proteins through any downstream mechanism present in the collecting duct cells. PPARγ would be located upstream of all the TZD & PGJ_2 dependent effects, therefore it would negate any activation of fibrotic markers. This was not the case and the exact mechanism(s) behind the Troglitazone induced EMT-like effects remains to be determined.

Our future approaches in characterizing the effects of TRO in the collecting duct will include the use of proteasome inhibitors and LiCl to verify whether a novel APC independent degradation pathway is involved in the decreasing levels of E-cadherin and β-catenin.

5.0 References

Ahmed, W., O. Ziouzenkova, et al. (2007). "PPARs and their metabolic modulation: new mechanisms for transcriptional regulation?" J Intern Med **262**(2): 184-98.

Annicotte, J. S., I. Iankova, et al. (2006). "Peroxisome proliferator-activated receptor gamma regulates E-cadherin expression and inhibits growth and invasion of prostate cancer." Mol Cell Biol **26**(20): 7561-74.

Aresu, L., M. P. Rastaldi, et al. (2007). "Epithelial-mesenchymal transition (EMT) of renal tubular cells in canine glomerulonephritis." Virchows Arch **451**(5): 937-42.

Atkins, K. B., C. A. Northcott, et al. (2005). "Effects of PPAR-gamma ligands on vascular smooth muscle marker expression in hypertensive and normal arteries." Am J Physiol Heart Circ Physiol **288**(1): H235-43.

Bakin, A. V., C. Rinehart, et al. (2002). "p38 mitogen-activated protein kinase is required for TGFbeta-mediated fibroblastic transdifferentiation and cell migration." J Cell Sci **115**(Pt 15): 3193-206.

Barish, G. D., V. A. Narkar, et al. (2006). "PPAR delta: a dagger in the heart of the metabolic syndrome." J Clin Invest **116**(3): 590-7.

Berger, J., M. D. Leibowitz, et al. (1999). "Novel peroxisome proliferator-activated receptor (PPAR) gamma and PPARdelta ligands produce distinct biological effects." J Biol Chem **274**(10): 6718-25.

Berger, J. and J. A. Wagner (2002). "Physiological and therapeutic roles of peroxisome proliferator-activated receptors." Diabetes Technol Ther **4**(2): 163-74.

Bishop-Bailey, D. and T. D. Warner (2003). "PPARgamma ligands induce prostaglandin production in vascular smooth muscle cells: indomethacin acts as a peroxisome proliferator-activated receptor-gamma antagonist." FASEB J **17**(13): 1925-7.

Bocca, C., F. Bozzo, et al. (2007). "Involvement of PPAR gamma and E-cadherin/beta-catenin pathway in the antiproliferative effect of conjugated linoleic acid in MCF-7 cells." Int J Cancer **121**(2): 248-56.

Boese, S. H., O. Aziz, et al. (2004). "Kinetics and regulation of a Ca2+-activated Cl- conductance in mouse renal inner medullary collecting duct cells." Am J Physiol Renal Physiol **286**(4): F682-92.

Borke, J. L., A. Costoff, et al. (1999). Essentials of Human Physiology. T. M. Nosek, Medical College of Georgia.

Brown, J. D. and J. Plutzky (2007). "Peroxisome proliferator-activated receptors as transcriptional nodal points and therapeutic targets." Circulation **115**(4): 518-33.

Bush, K. T., T. Tsukamoto, et al. (2000). "Selective degradation of E-cadherin and dissolution of E-cadherin-catenin complexes in epithelial ischemia." Am J Physiol Renal Physiol **278**(5): F847-52.

Butt, M. J., A. F. Tarantal, et al. (2007). "Collecting duct epithelial-mesenchymal transition in fetal urinary tract obstruction." Kidney Int **72**(8): 936-44.

Cha, D. R., X. Zhang, et al. (2007). "Peroxisome proliferator activated receptor alpha/gamma dual agonist tesaglitazar attenuates diabetic nephropathy in db/db mice." Diabetes **56**(8): 2036-45.

Chen, L., B. M. Necela, et al. (2006). "Peroxisome proliferator-activated receptor gamma promotes epithelial to mesenchymal transformation by Rho GTPase-dependent activation of ERK1/2." J Biol Chem **281**(34): 24575-87.

Chen, X., R. B. Halberg, et al. (2008). "Intestinal adenomagenesis involves core molecular signatures of the epithelial-mesenchymal transition." J Mol Histol **39**(3): 283-94.

Cheng, H. C., T. C. Ho, et al. (2008). "Troglitazone suppresses transforming growth factor beta-mediated fibrogenesis in retinal pigment epithelial cells." Mol Vis **14**: 95-104.

Chou, F. S., P. S. Wang, et al. (2007). "Effects of thiazolidinediones on differentiation, proliferation, and apoptosis." Mol Cancer Res **5**(6): 523-30.

Choy, L., J. Skillington, et al. (2000). "Roles of autocrine TGF-beta receptor and Smad signalling in adipocyte differentiation." J Cell Biol **149**(3): 667-82.

Clapp, W. L., K. M. Madsen, et al. (1987). "Intercalated cells of the rat inner medullary collecting duct." Kidney Int **31**(5): 1080-7.

Clay, C. E., A. M. Namen, et al. (2001). "Magnitude of peroxisome proliferator-activated receptor-gamma activation is associated

with important and seemingly opposite biological responses in breast cancer cells." J Investig Med **49**(5): 413-20.

Desclozeaux, M., J. Venturato, et al. (2008). "Active Rab11 and functional recycling endosome are required for E-cadherin trafficking and lumen formation during epithelial morphogenesis." Am J Physiol Cell Physiol **295**(2): C545-56.

Dillard, A. C. and M. A. Lane (2007). "Retinol decreases beta-catenin protein levels in retinoic acid-resistant colon cancer cell lines." Mol Carcinog **46**(4): 315-29.

Dillard, A. C. and M. A. Lane (2008). "Retinol Increases beta-catenin-RXRalpha binding leading to the increased proteasomal degradation of beta-catenin and RXRalpha." Nutr Cancer **60**(1): 97-108.

Djouadi, F. and J. Bastin (2001). "PPARalpha gene expression in the developing rat kidney: role of glucocorticoids." J Am Soc Nephrol **12**(6): 1197-203.

Drees, F., S. Pokutta, et al. (2005). "Alpha-catenin is a molecular switch that binds E-cadherin-beta-catenin and regulates actin-filament assembly." Cell **123**(5): 903-15.

Efrati, S., S. Berman, et al. (2007). "PPAR-gamma activation inhibits angiotensin II synthesis, apoptosis, and proliferation of mesangial cells from spontaneously hypertensive rats." Nephron Exp Nephrol **106**(4): e107-12.

Fajas, L., J. C. Fruchart, et al. (1998). "PPARgamma3 mRNA: a distinct PPARgamma mRNA subtype transcribed from an independent promoter." FEBS Lett **438**(1-2): 55-60.

Falin, R., I. E. Veizis, et al. (2005). "A role for ERK1/2 in EGF- and ATP-dependent regulation of amiloride-sensitive sodium absorption." Am J Physiol Cell Physiol **288**(5): C1003-11.

Fan, L., A. Sebe, et al. (2007). "Cell contact-dependent regulation of epithelial-myofibroblast transition via the rho-rho kinase-phospho-myosin pathway." Mol Biol Cell **18**(3): 1083-97.

Feige, J. N., L. Gelman, et al. (2006). "From molecular action to physiological outputs: peroxisome proliferator-activated receptors are nuclear receptors at the crossroads of key cellular functions." Prog Lipid Res **45**(2): 120-59.

Feinstein, D. L., A. Spagnolo, et al. (2005). "Receptor-independent actions of PPAR thiazolidinedione agonists: is mitochondrial function the key?" Biochem Pharmacol **70**(2): 177-88.

Gardner, O. S., B. J. Dewar, et al. (2003). "Dependence of peroxisome proliferator-activated receptor ligand-induced mitogen-activated protein kinase signalling on epidermal growth factor receptor transactivation." J Biol Chem **278**(47): 46261-9.

Giral, H., R. Villa-Bellosta, et al. (2007). "Cytotoxicity of peroxisome proliferator-activated receptor alpha and gamma agonists in renal proximal tubular cell lines." Toxicol In Vitro **21**(6): 1066-76.

Goetze, S., U. Kintscher, et al. (2001). "Peroxisome proliferator-activated receptor-gamma ligands inhibit nuclear but not cytosolic extracellular signal-regulated kinase/mitogen-activated protein kinase-regulated steps in vascular smooth muscle cell migration." J Cardiovasc Pharmacol **38**(6): 909-21.

Gradl, D., M. Kuhl, et al. (1999). "The Wnt/Wg signal transducer beta-catenin controls fibronectin expression." Mol Cell Biol **19**(8): 5576-87.

Guan, Y., C. Hao, et al. (2005). "Thiazolidinediones expand body fluid volume through PPARgamma stimulation of ENaC-mediated renal salt absorption." Nat Med **11**(8): 861-6.

Guan, Y., Y. Zhang, et al. (1997). "Expression of peroxisome proliferator-activated receptors in urinary tract of rabbits and humans." Am J Physiol **273**(6 Pt 2): F1013-22.

Guo, B., D. Koya, et al. (2004). "Peroxisome proliferator-activated receptor-gamma ligands inhibit TGF-beta 1-induced fibronectin expression in glomerular mesangial cells." Diabetes **53**(1): 200-8.

Guo, W., J. Flanagan, et al. (2008). "The effects of myostatin on adipogenic differentiation of human bone marrow-derived mesenchymal stem cells are mediated through cross-communication between Smad3 and Wnt/beta-catenin signalling pathways." J Biol Chem **283**(14): 9136-45.

Han, K. H., H. Y. Kim, et al. (2007). "Effects of ischemia-reperfusion injury on renal ammonia metabolism and the collecting duct." Am J Physiol Renal Physiol **293**(4): F1342-54.

Han, S., J. D. Ritzenthaler, et al. (2005). "Peroxisome proliferator-activated receptor-gamma ligands suppress fibronectin gene expression in human lung carcinoma cells: involvement of both CRE and Sp1." Am J Physiol Lung Cell Mol Physiol **289**(3): L419-28.

Hansen, B. C. (1999). "The metabolic syndrome X." Ann N Y Acad Sci **892**: 1-24.

Hao, G. H., X. L. Niu, et al. (2008). "Agonists at PPAR-gamma suppress angiotensin II-induced production of plasminogen activator inhibitor-1 and extracellular matrix in rat cardiac fibroblasts." Br J Pharmacol **153**(7): 1409-19.

Hauser, S., G. Adelmant, et al. (2000). "Degradation of the peroxisome proliferator-activated receptor gamma is linked to ligand-dependent activation." J Biol Chem **275**(24): 18527-33.

Haverty, T. P., C. J. Kelly, et al. (1988). "Characterization of a renal tubular epithelial cell line which secretes the autologous target antigen of autoimmune experimental interstitial nephritis." J Cell Biol **107**(4): 1359-68.

Hellman, N. E., J. Spector, et al. (2008). "Matrix metalloproteinase 13 (MMP13) and tissue inhibitor of matrix metalloproteinase 1 (TIMP1), regulated by the MAPK pathway, are both necessary for Madin-Darby canine kidney tubulogenesis." J Biol Chem **283**(7): 4272-82.

Hoorn, E. J., T. Pisitkun, et al. (2008). "Proteomic approaches for the study of cell signalling in the renal collecting duct." Contrib Nephrol **160**: 172-85.

Husted, R. F., R. D. Sigmund, et al. (2000). "Mechanisms of inactivation of the action of aldosterone on collecting duct by TGF-beta." Am J Physiol Renal Physiol **278**(3): F425-33.

Husted, R. F. and J. B. Stokes (1996). "Separate regulation of Na+ and anion transport by IMCD: location, aldosterone, hypertonicity, TGF-beta 1, and cAMP." Am J Physiol **271**(2 Pt 2): F433-9.

Ide, T., K. Egan, et al. (2003). "Activation of nuclear receptors by prostaglandins." Thromb Res **110**(5-6): 311-5.

Iglarz, M., R. M. Touyz, et al. (2003). "Peroxisome proliferator-activated receptor-alpha and receptor-gamma activators prevent cardiac fibrosis in mineralocorticoid-dependent hypertension." Hypertension **42**(4): 737-43.

Ito, O., Y. Nakamura, et al. (2006). "Expression of cytochrome P-450 4 enzymes in the kidney and liver: regulation by PPAR and species-difference between rat and human." Mol Cell Biochem **284**(1-2): 141-8.

Ivanova, L., M. J. Butt, et al. (2008). "Mesenchymal transition in kidney collecting duct epithelial cells." Am J Physiol Renal Physiol **294**(5): F1238-48.

Izzedine, H., V. Launay-Vacher, et al. (2005). "PPAR-gamma-agonists' renal effects." Minerva Urol Nefrol **57**(4): 247-60.

Javle, M. M., J. F. Gibbs, et al. (2007). "Epithelial-mesenchymal transition (EMT) and activated extracellular signal-regulated kinase (p-Erk) in surgically resected pancreatic cancer." Ann Surg Oncol **14**(12): 3527-33.

Jo, S. H., C. Yang, et al. (2006). "Peroxisome proliferator-activated receptor gamma promotes lymphocyte survival through its actions on cellular metabolic activities." J Immunol **177**(6): 3737-45.

Kang, D. S., C. H. Kwon, et al. (2006). "15-deoxy-Delta12,14-prostaglandin J2 induces renal epithelial cell death through NF-kappaB-dependent and MAPK-independent mechanism." Toxicol Appl Pharmacol **216**(3): 426-35.

Kanjanabuch, T., L. J. Ma, et al. (2007). "PPAR-gamma agonist protects podocytes from injury." Kidney Int **71**(12): 1232-9.

Kim, S. H., C. I. Yoo, et al. (2006). "Activation of peroxisome proliferator-activated receptor-gamma (PPARgamma) induces cell death through MAPK-dependent mechanism in osteoblastic cells." Toxicol Appl Pharmacol **215**(2): 198-207.

Kimura, H., X. Li, et al. (2008). "A natural PPAR-gamma agonist, 15-deoxy-delta 12,14-prostaglandin J2, may act as an enhancer of PAI-1 in human proximal renal tubular cells under hypoxic and inflammatory conditions." Nephrol Dial Transplant **23**(8): 2496-503.

Kispert, A., S. Vainio, et al. (1998). "Wnt-4 is a mesenchymal signal for epithelial transformation of metanephric mesenchyme in the developing kidney." Development **125**(21): 4225-34.

Kizer, N. L., B. Lewis, et al. (1995). "Electrogenic sodium absorption and chloride secretion by an inner medullary collecting duct cell line (mIMCD-K2)." Am J Physiol **268**(2 Pt 2): F347-55.

Kota, B. P., T. H. Huang, et al. (2005). "An overview on biological mechanisms of PPARs." Pharmacol Res **51**(2): 85-94.

Kumar, R. and E. B. Thompson (1999). "The structure of the nuclear hormone receptors." Steroids **64**(5): 310-9.

Kume, S., T. Uzu, et al. (2007). "Role of altered renal lipid metabolism in the development of renal injury induced by a high-fat diet." J Am Soc Nephrol **18**(10): 2715-23.

Labbe, E., A. Letamendia, et al. (2000). "Association of Smads with lymphoid enhancer binding factor 1/T cell-specific factor mediates cooperative signalling by the transforming growth factor-beta and wnt pathways." Proc Natl Acad Sci U S A **97**(15): 8358-63.

Lee, G., F. Elwood, et al. (2002). "T0070907, a selective ligand for peroxisome proliferator-activated receptor gamma, functions as an antagonist of biochemical and cellular activities." J Biol Chem **277**(22): 19649-57.

Lee, S. J., M. S. Kim, et al. (2008). "15-Deoxy-delta 12,14-prostaglandin J2 induces apoptosis via JNK-mediated mitochondrial pathway in osteoblastic cells." Toxicology **248**(2-3): 121-9.

Leesnitzer, L. M., D. J. Parks, et al. (2002). "Functional consequences of cysteine modification in the ligand binding sites of peroxisome proliferator activated receptors by GW9662." Biochemistry **41**(21): 6640-50.

Lehmann, J. M., L. B. Moore, et al. (1995). "An antidiabetic thiazolidinedione is a high affinity ligand for peroxisome proliferator-activated receptor gamma (PPAR gamma)." J Biol Chem **270**(22): 12953-6.

Leibowitz, M. D., R. J. Ardecky, et al. (2006). "Biological characterization of a heterodimer-selective retinoid X receptor modulator: potential benefits for the treatment of type 2 diabetes." Endocrinology **147**(2): 1044-53.

Li, M., T. W. Lee, et al. (2006). "Apoptosis induced by troglitazone is both peroxisome proliferator-activated receptor-gamma- and ERK-dependent in human non-small lung cancer cells." J Cell Physiol **209**(2): 428-38.

Li, Y., Y. S. Kang, et al. (2008). "Epithelial-to-mesenchymal transition is a potential pathway leading to podocyte dysfunction and proteinuria." Am J Pathol **172**(2): 299-308.

Li, Y., X. Wen, et al. (2006). "hepatocyte growth factor is a downstream effector that mediates the antifibrotic action of peroxisome proliferator-activated receptor-gamma agonists." J Am Soc Nephrol **17**(1): 54-65.

Liu, J. and S. R. Farmer (2004). "Regulating the balance between peroxisome proliferator-activated receptor gamma and beta-catenin signalling during adipogenesis. A glycogen synthase kinase 3beta phosphorylation-defective mutant of beta-catenin inhibits expression of a subset of adipogenic genes." J Biol Chem **279**(43): 45020-7.

Liu, J., J. Stevens, et al. (2001). "Siah-1 mediates a novel beta-catenin degradation pathway linking p53 to the adenomatous polyposis coli protein." Mol Cell **7**(5): 927-36.

Liu, J., H. Wang, et al. (2006). "Functional interaction between peroxisome proliferator-activated receptor gamma and beta-catenin." Mol Cell Biol **26**(15): 5827-37.

Mandal, M., J. N. Myers, et al. (2008). "Epithelial to mesenchymal transition in head and neck squamous carcinoma: association of Src activation with E-cadherin down-regulation, vimentin expression, and aggressive tumor features." Cancer **112**(9): 2088-100.

Masszi, A., L. Fan, et al. (2004). "Integrity of cell-cell contacts is a critical regulator of TGF-beta 1-induced epithelial-to-myofibroblast transition: role for beta-catenin." Am J Pathol **165**(6): 1955-67.

McEneaney, V., B. J. Harvey, et al. (2007). "Aldosterone rapidly activates protein kinase D via a mineralocorticoid receptor/EGFR trans-activation pathway in the M1 kidney CCD cell line." J Steroid Biochem Mol Biol **107**(3-5): 180-90.

Michalik, L., J. Auwerx, et al. (2006). "International Union of Pharmacology. LXI. Peroxisome proliferator-activated receptors." Pharmacol Rev **58**(4): 726-41.

Milam, J. E., V. G. Keshamouni, et al. (2008). "PPAR-gamma agonists inhibit profibrotic phenotypes in human lung fibroblasts and bleomycin-induced pulmonary fibrosis." Am J Physiol Lung Cell Mol Physiol **294**(5): L891-901.

Mulholland, D. J., S. Dedhar, et al. (2005). "Interaction of nuclear receptors with the Wnt/beta-catenin/Tcf signalling axis: Wnt you like to know?" Endocr Rev **26**(7): 898-915.

Nelson, W. J. and R. Nusse (2004). "Convergence of Wnt, beta-catenin, and cadherin pathways." Science **303**(5663): 1483-7.

Panchapakesan, U., C. A. Pollock, et al. (2004). "The effect of high glucose and PPAR-gamma agonists on PPAR-gamma expression and function in HK-2 cells." Am J Physiol Renal Physiol **287**(3): F528-34.

Panchapakesan, U., S. Sumual, et al. (2005). "PPARgamma agonists exert antifibrotic effects in renal tubular cells exposed to high glucose." Am J Physiol Renal Physiol **289**(5): F1153-8.

Peng, Y., H. Liu, et al. (2006). "Troglitazone inhibits synthesis of transforming growth factor-beta1 and reduces matrix production in human peritoneal mesothelial cells." Nephrology (Carlton) **11**(6): 516-23.

Perez, A., A. M. van Heeckeren, et al. (2008). "Peroxisome proliferator-activated receptor-gamma in cystic fibrosis lung epithelium." Am J Physiol Lung Cell Mol Physiol **295**(2): L303-13.

Prozialeck, W. C., P. C. Lamar, et al. (2004). "Differential expression of E-cadherin, N-cadherin and beta-catenin in proximal and distal segments of the rat nephron." BMC Physiol **4**: 10.

Qiao, L., Y. Dai, et al. (2008). "Loss of XIAP sensitizes colon cancer cells to PPARgamma independent antitumor effects of troglitazone and 15-PGJ2." Cancer Lett **268**(2): 260-71.

Qin, Y., X. W. Li, et al. (2006). "[Effects of rosiglitazone on the expression connective tissue growth factor in tubulointerstitium in KKA(y) mice]." Zhongguo Yi Xue Ke Xue Yuan Xue Bao **28**(6): 817-21.

Radisky, D. C., P. A. Kenny, et al. (2007). "Fibrosis and cancer: do myofibroblasts come also from epithelial cells via EMT?" J Cell Biochem **101**(4): 830-9.

Reynolds, A. B. and R. H. Carnahan (2004). "Regulation of cadherin stability and turnover by p120ctn: implications in disease and cancer." Semin Cell Dev Biol **15**(6): 657-63.

Rhyu, D. Y., Y. Yang, et al. (2005). "Role of reactive oxygen species in TGF-beta1-induced mitogen-activated protein kinase activation and epithelial-mesenchymal transition in renal tubular epithelial cells." J Am Soc Nephrol **16**(3): 667-75.

Rosa, A. O., J. Egea, et al. (2008). "Neuroprotective effect of the new thiadiazolidinone NP00111 against oxygen-glucose deprivation in rat hippocampal slices: implication of ERK1/2 and PPARgamma receptors." Exp Neurol **212**(1): 93-9.

Ryves, W. J. and A. J. Harwood (2001). "Lithium inhibits glycogen synthase kinase-3 by competition for magnesium." Biochem Biophys Res Commun **280**(3): 720-5.

Saad, S., D. J. Gottlieb, et al. (2002). "Cancer cell-associated fibronectin induces release of matrix metalloproteinase-2 from normal fibroblasts." Cancer Res **62**(1): 283-9.

Sam, R., L. Wanna, et al. (2006). "Glomerular epithelial cells transform to myofibroblasts: early but not late removal of TGF-beta1 reverses transformation." Transl Res **148**(3): 142-8.

Schiefelbein, D., O. Seitz, et al. (2008). "Keratinocyte-derived VEGF biosynthesis represents a pleiotropic side effect of PPAR{gamma} agonist troglitazone but not rosiglitazone and involves activation of p38 MAPK: implications for diabetes-impaired skin repair." Mol Pharmacol.

Schramek, H., E. Feifel, et al. (2003). "Loss of active MEK1-ERK1/2 restores epithelial phenotype and morphogenesis in transdifferentiated MDCK cells." Am J Physiol Cell Physiol **285**(3): C652-61.

Sharma, C., A. Pradeep, et al. (2004). "Peroxisome proliferator-activated receptor gamma activation can regulate beta-catenin levels via a proteasome-mediated and adenomatous polyposis coli-independent pathway." J Biol Chem **279**(34): 35583-94.

Shimizu, M. and H. Moriwaki (2008). "Synergistic Effects of PPARgamma Ligands and Retinoids in Cancer Treatment." PPAR Res **2008**: 181047.

Singh, N., R. Webb, et al. (2005). "The PPAR-gamma activator, Rosiglitazone, inhibits actin polymerisation in monocytes: involvement of Akt and intracellular calcium." Biochem Biophys Res Commun **333**(2): 455-62.

Stokes, J. B. (2000). "Physiologic resistance to the action of aldosterone." Kidney Int **57**(4): 1319-23.

Stoos, B. A., A. Naray-Fejes-Toth, et al. (1991). "Characterization of a mouse cortical collecting duct cell line." Kidney Int **39**(6): 1168-75.

Surendran, K., S. P. McCaul, et al. (2002). "A role for Wnt-4 in renal fibrosis." Am J Physiol Renal Physiol **282**(3): F431-41.

Takada, I., M. Mihara, et al. (2007). "A histone lysine methyltransferase activated by non-canonical Wnt signalling suppresses PPAR-gamma transactivation." Nat Cell Biol **9**(11): 1273-85.

Takata, K., Y. Tajika, et al. (2004). "Molecular mechanisms and drug development in aquaporin water channel diseases: water channel aquaporin-2 of kidney collecting duct cells." J Pharmacol Sci **96**(3): 255-9.

Takeji, M., T. Moriyama, et al. (2006). "Smooth muscle alpha-actin deficiency in myofibroblasts leads to enhanced renal tissue fibrosis." J Biol Chem **281**(52): 40193-200.

Thews, O., C. Lambert, et al. (2007). "Impact of therapeutically induced reactive oxygen species and radical scavenging by alpha-tocopherol on tumor cell adhesion." Oncol Rep **18**(4): 965-71.

Tian, Y. C., Y. C. Chen, et al. (2007). "Epidermal growth factor and transforming growth factor-beta1 enhance HK-2 cell migration through a synergistic increase of matrix metalloproteinase and sustained activation of ERK signalling pathway." Exp Cell Res **313**(11): 2367-77.

Tian, Y. C. and A. O. Phillips (2002). "Interaction between the transforming growth factor-beta type II receptor/Smad pathway and beta-catenin during transforming growth factor-beta1-mediated adherens junction disassembly." Am J Pathol **160**(5): 1619-28.

Tontonoz, P., E. Hu, et al. (1994). "mPPAR gamma 2: tissue-specific regulator of an adipocyte enhancer." Genes Dev **8**(10): 1224-34.

Tsujie, M., S. Nakamori, et al. (2003). "Thiazolidinediones inhibit growth of gastrointestinal, biliary, and pancreatic adenocarcinoma cells through activation of the peroxisome proliferator-activated receptor gamma/retinoid X receptor alpha pathway." Exp Cell Res **289**(1): 143-51.

Turturro, F., R. Oliver, 3rd, et al. (2007). "Troglitazone and pioglitazone interactions via PPAR-gamma-independent and -dependent pathways in regulating physiological responses in renal tubule-derived cell lines." Am J Physiol Cell Physiol **292**(3): C1137-46.

Uawithya, P., T. Pisitkun, et al. (2008). "Transcriptional profiling of native inner medullary collecting duct cells from rat kidney." Physiol Genomics **32**(2): 229-53.

Uttamsingh, S., X. Bao, et al. (2008). "Synergistic effect between EGF and TGF-beta1 in inducing oncogenic properties of intestinal epithelial cells." Oncogene **27**(18): 2626-34.

Wang, W., F. Liu, et al. (2007). "Peroxisome proliferator-activated receptor-gamma (PPAR-gamma) agonists attenuate the profibrotic response induced by TGF-beta1 in renal interstitial fibroblasts." Mediators Inflamm **2007**: 62641.

Wilkins-Port, C. E. and P. J. Higgins (2007). "Regulation of extracellular matrix remodeling following transforming growth factor-beta1/epidermal growth factor-stimulated epithelial-

mesenchymal transition in human premalignant keratinocytes." Cells Tissues Organs **185**(1-3): 116-22.

Wu, Z., L. Yang, et al. (2007). "Detection of epithelial to mesenchymal transition in airways of a bleomycin induced pulmonary fibrosis model derived from an alpha-smooth muscle actin-Cre transgenic mouse." Respir Res **8**: 1.

Wynn, T. A. (2008). "Cellular and molecular mechanisms of fibrosis." J Pathol **214**(2): 199-210.

Xiao, J. H., C. Ghosn, et al. (2003). "Adenomatous polyposis coli (APC)-independent regulation of beta-catenin degradation via a retinoid X receptor-mediated pathway." J Biol Chem **278**(32): 29954-62.

Xie, L., B. K. Law, et al. (2004). "Activation of the Erk pathway is required for TGF-beta1-induced EMT in vitro." Neoplasia **6**(5): 603-10.

Xing, B., T. Xin, et al. (2008). "Pioglitazone inhibition of lipopolysaccharide-induced nitric oxide synthase is associated with altered activity of p38 MAP kinase and PI3K/Akt." J Neuroinflammation **5**: 4.

Yang, C., S. H. Jo, et al. (2007). "Activation of peroxisome proliferator-activated receptor gamma contributes to the survival of T lymphoma cells by affecting cellular metabolism." Am J Pathol **170**(2): 722-32.

Yang, T., D. E. Michele, et al. (1999). "Expression of peroxisomal proliferator-activated receptors and retinoid X receptors in the kidney." Am J Physiol **277**(6 Pt 2): F966-73.

Yang, Y., X. Pan, et al. (2006). "Regulation of transforming growth factor-beta 1-induced apoptosis and epithelial-to-mesenchymal transition by protein kinase A and signal transducers and activators of transcription 3." Cancer Res **66**(17): 8617-24.

Zafiriou, S., S. R. Stanners, et al. (2005). "Pioglitazone inhibits cell growth and reduces matrix production in human kidney fibroblasts." J Am Soc Nephrol **16**(3): 638-45.

Zhai, Y., R. Wu, et al. (2002). "Role of beta-catenin/T-cell factor-regulated genes in ovarian endometrioid adenocarcinomas." Am J Pathol **160**(4): 1229-38.

Zhang, H., A. Zhang, et al. (2005). "Collecting duct-specific deletion of peroxisome proliferator-activated receptor gamma blocks

thiazolidinedione-induced fluid retention." Proc Natl Acad Sci U S A **102**(26): 9406-11.

6.0 Appendix

6.1 Chemical list

- 15-deoxy-Prostaglandin J2 (cayman chemical cat#18570)
- AlexaFluor Phalloidin 488nm was a gift from Dr. Chris Kennedy (University of Ottawa)
- Anti-Fibronectin (Sigma F-3648)
- Anti-mouse Ig, fluorescein linked (Amersham N1031)
- Anti-Mouse IgG (H+L), HRP Conjugate (Promega W4021)
- Anti-Rabbit IgG (H+L), HRP Conjugate (Promega W4011)
- Anti-α-catenin (Sigma)
- Anti-β-catenin (R&D, Sigma)
- Donkey Anti-Goat HRP (Promega V805A)
- Epidermal Growth Factor (EGF) (Sigma)
- Fluoromount G (Electron Microscopy Sciences cat# 17984-25)
- Goat Anti-Rat IgG, Peroxidase-conjugated (Jackson ImmunoResearch Lab T12-035-003)
- GSK-3 blocker SB-216763 (Sigma)
- GW9662 (cayman chemical cat# 70785)
- Monoclonal Anti-Uvomorulin/E-cadherin (Sigma U3254-.2ML)
- Monoclonal Anti-α-SMA (Sigma A-5228)
- p-38 & total p38 anti-rabbit was a gift from Dr. Kevin Burns (University of Ottawa)
- p-erk1/2 & total erk1/2 was a gift from Dr. Kevin Burns (University of Ottawa)
- Ployfect Transfection Reagent (Qiagen)
- PPARγ (E-8): sc-7273 (Santa Cruz Biotechnology)
- Recombinant human TGF-β1 (R&D Systems CAT# 240-b)
- T0070907 (cayman chemical)
- Total smad2&3 (R&D Systems)
- Troglitazone (Sigma T2573-5MG)

6.2 PPARγ insert characterization

In order to validate the integrity of the pcDNA vectors, digests were ran to ensure a proper insertion of PPARγ. Undigested samples were run beside the pcDNA vectors.

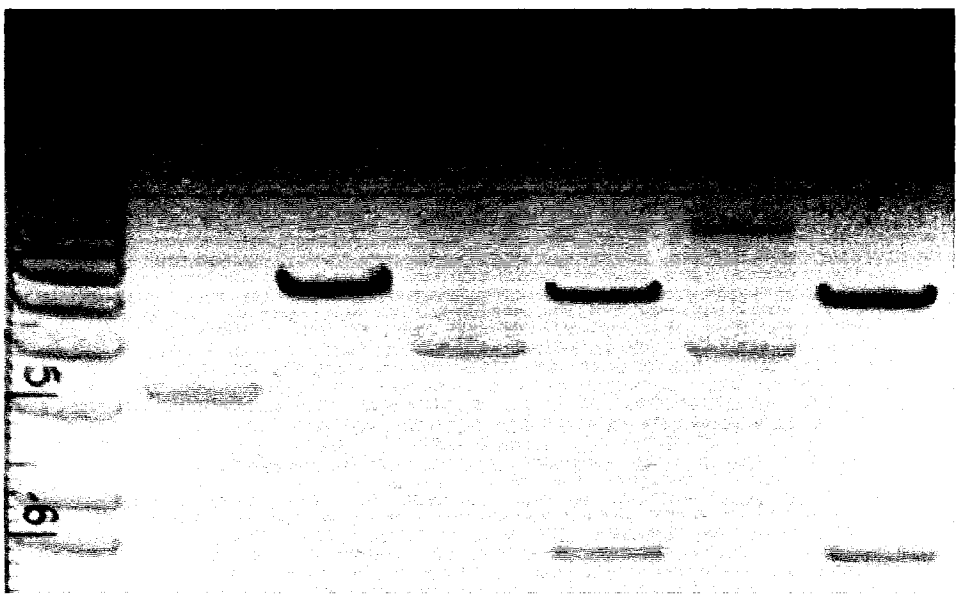

	pcDNA		pcDNA-PPARγ		pcDNA-PPARγ E499Q	
XhoI	-	+	-	+	-	+
HindIII	-	+	-	+	-	+

Fig. 35 - Restriction Enzyme digest of pcDNA PPARγ vectors.

pcDNA, pcDNA-PPARγ, and pcDNA-PPARγ EQ4994 vectors were digested with XhoI and HindIII. 5-10μL of digested sample was removed, added to DNA loading buffer and separated by electrophoresis on a 1% agarose gel. The bands were visualized with an Alpha Innotec Alpha Imager under the ethidium bromide filter.